

**UNIVERSIDAD DE INVESTIGACIÓN DE TECNOLOGÍA
EXPERIMENTAL YACHAY**

ESCUELA DE CIENCIAS DE LA TIERRA, ENERGÍA Y AMBIENTE

**CHARACTERIZATION OF THE DEFORMATION IN THE SAN MIGUEL
FORMATION WITHIN THE GUAYLLABAMBA BASIN**

Trabajo de integración curricular presentado como requisito para la obtención del
título de Geólogo

Autor:

Michael Angelo Andramuño González

Tutor:

Ph.D. Anna Elizabeth Foster

Co-tutor:

Ph.D. Rafael Vladimir Almeida González

Urcuquí, 17 de agosto de 2022

SECRETARÍA GENERAL
ESCUELA DE CIENCIAS DE LA TIERRA, ENERGÍA Y AMBIENTE
CARRERA DE GEOLOGÍA
ACTA DE DEFENSA No. UITEY-GEO-2022-00009-AD

En la ciudad de San Miguel de Urcuquí, Provincia de Imbabura, a los 17 días del mes de agosto de 2022, a las 10:00 horas, en el Aula S_CAN de la Universidad de Investigación de Tecnología Experimental Yachay y ante el Tribunal Calificador, integrado por los docentes:

Presidente Tribunal de Defensa	Dr. VAZQUEZ TASET, YANIEL MISAEL , Ph.D.
Miembro No Tutor	Dr. TORO ALAVA, JORGE EDUARDO , Ph.D.
Tutor	Dra. FOSTER ANNA ELIZABETH , Ph.D.

Se presenta el(la) señor(ita) estudiante **ANDRAMUÑO GONZALEZ, MICHAEL ANGELO**, con cédula de identidad No. **0931662829**, de la **ESCUELA DE CIENCIAS DE LA TIERRA, ENERGÍA Y AMBIENTE**, de la Carrera de **GEOLOGÍA**, aprobada por el Consejo de Educación Superior (CES), mediante Resolución **RPC-SE-10-No.031-2016**, con el objeto de rendir la sustentación de su trabajo de titulación denominado: **Characterization of the deformation in the San Miguel formation within the Guayllabamba basin**, previa a la obtención del título de **GEÓLOGO/A**.

El citado trabajo de titulación, fue debidamente aprobado por el(los) docente(s):

Tutor	Dra. FOSTER ANNA ELIZABETH , Ph.D.
--------------	------------------------------------

Y recibió las observaciones de los otros miembros del Tribunal Calificador, las mismas que han sido incorporadas por el(la) estudiante.

Previamente cumplidos los requisitos legales y reglamentarios, el trabajo de titulación fue sustentado por el(la) estudiante y examinado por los miembros del Tribunal Calificador. Escuchada la sustentación del trabajo de titulación, que integró la exposición de el(la) estudiante sobre el contenido de la misma y las preguntas formuladas por los miembros del Tribunal, se califica la sustentación del trabajo de titulación con las siguientes calificaciones:

Tipo	Docente	Calificación
Presidente Tribunal De Defensa	Dr. VAZQUEZ TASET, YANIEL MISAEL , Ph.D.	9,4
Tutor	Dra. FOSTER ANNA ELIZABETH , Ph.D.	9,5
Miembro Tribunal De Defensa	Dr. TORO ALAVA, JORGE EDUARDO , Ph.D.	9,2

Lo que da un promedio de: **9.4 (Nueve punto Cuatro)**, sobre 10 (diez), equivalente a: **APROBADO**

Para constancia de lo actuado, firman los miembros del Tribunal Calificador, el/la estudiante y el/la secretario ad-hoc.

ANDRAMUÑO GONZALEZ, MICHAEL ANGELO
Estudiante



Firmado electrónicamente por:
MICHAEL ANGELO ANDRAMUNO GONZALEZ

Dr. VAZQUEZ TASET, YANIEL MISAEL , Ph.D.
Presidente Tribunal de Defensa

YANIEL MISAEL VAZQUEZ TASET



Dra. FOSTER ANNA ELIZABETH , Ph.D.
Tutor

ANNA ELIZABETH FOSTER

Digitally signed by ANNA ELIZABETH FOSTER
Date: 2022.08.18 10:53:49 -07'00'

Dr. TORO ALAVA, JORGE EDUARDO , Ph.D.
Miembro No Tutor

JORGE EDUARDO TORO ALAVA

Firmado digitalmente por JORGE EDUARDO TORO ALAVA
Fecha: 2022.08.22 15:56:40 -05'00'

TERÁN ROSALES, ANDREA YOLANDA
Secretario Ad-hoc



Firmado electrónicamente por:
ANDREA YOLANDA TERAN ROSALES

AUTORÍA

Yo, **MICHAEL ANGELO ANDRAMUÑO GONZÁLEZ**, con cédula de identidad 0931662829, declaro que las ideas, juicios, valoraciones, interpretaciones, consultas bibliográficas, definiciones y conceptualizaciones expuestas en el presente trabajo; así como, los procedimientos y herramientas utilizadas en la investigación, son de absoluta responsabilidad de el/la autora (a) del trabajo de integración curricular. Así mismo, me acojo a los reglamentos internos de la Universidad de Investigación de Tecnología Experimental Yachay.

Urcuquí, agosto de 2022.

Michael Angelo Andramuño González
CI:0931662829

AUTORIZACIÓN DE PUBLICACIÓN

Yo, **MICHAEL ANGELO ANDRAMUÑO GONZÁLEZ**, con cédula de identidad 0931662829, cedo a la Universidad de Investigación de Tecnología Experimental Yachay, los derechos de publicación de la presente obra, sin que deba haber un reconocimiento económico por este concepto. Declaro además que el texto del presente trabajo de titulación no podrá ser cedido a ninguna empresa editorial para su publicación u otros fines, sin contar previamente con la autorización escrita de la Universidad.

Asimismo, autorizo a la Universidad que realice la digitalización y publicación de este trabajo de integración curricular en el repositorio virtual, de conformidad a lo dispuesto en el Art. 144 de la Ley Orgánica de Educación Superior

Urcuquí, agosto de 2022.

Michael Angelo Andramuño González
CI:0931662829

DEDICATORIA

Dedico este trabajo a mis padres quienes me han dado apoyo incondicional durante toda mi carrera universitaria quienes me han inculcado la importancia del esfuerzo y el trabajo duro.

AGRADECIMIENTOS

Agradezco a todos los profesores (Elisa, Celine, Yaniel, Alejandra, Luis Felipe, entre otros) que me he encontrado durante la travesía de estudiar esta carrera universitaria porque me enseñaron el valor y la importancia de hacer ciencia de calidad. También me enseñaron que no importa ser un excelente profesional si no soy una gran persona. Sin embargo, quiero agradecer especialmente a Rafael Almeida, Anna Foster, German Martin, Karla Freire y José Luis Flores.

Agradezco principalmente a Rafael Almeida quien me ha ayudado a darle dirección a este proyecto, me ha asesorado en la parte académica, me ha acompañado en campo, me inculcó la pasión por la Geología de campo y me ha dado ánimos cuando parecía que ya me rendía en la escritura de este trabajo. También agradezco a Anna Foster por ser la persona que me ha representado dentro de la institución como mi Tutora y me ha ayudado a solucionar el papeleo engorroso necesario para llevar a cabo este proyecto. Le doy gracias a German Martin porque me dio consejos de geología y de vida, me acompañó al campo, me compartió información de su trabajo previo en Guayllabamba. Además, agradezco a Karla Freire por su ayuda y asesoramiento en la creación del modelo 3D y la fotogrametría. Finalmente le doy muchas gracias a José Luis Flores que me ayudó con el vuelo del dron y la captura de las fotos para la creación del modelo 3D.

Por otro lado, quiero agradecer a la Familia Bosque Narvaez quienes me abrieron las puertas de su finca y de su vida. Muchas gracias porque ellos hicieron que acampar en Guayllabamba se sienta como estar en casa. También agradezco a los amigas y amigos que hice mientras estuve en Yachay Tech porque alegraron mi vida universitaria. Aunque algunas de estas amistades hoy ya no sigan siendo parte de mi vida, se les agradece por lo que me aportaron y por el cariño que me brindaron. A las amistades que aún están ahí las llevo con un gran aprecio en el corazón: Marjorie, Karla, Nadine, Joseline, Henry, Paul, Lester y especialmente a Alexandra Oña quien me motivó mucho, me acompañó muchas horas: algunas en el campo y muchísimas más en la cotidianidad de la vida.

Finalmente, agradezco a Miguel Andramuño por ser mi papá y mi gran amigo. También agradezco a Elisa González por ser mi mamá y ser una gran amiga. Gracias a los dos por sus consejos, por las muchas horas de apoyo, y sobre todo por el amor y cariño que me han dado siempre.

RESUMEN

Ecuador está principalmente dividido en tres regiones geológicas: la Cordillera Oeste, la Cordillera Real, y el valle Interandino. El Valle Interandino está conformado por algunas cuencas sedimentarias tales como: Chota, Guayllabamba, Ambato-Latacunga, Alausí-Riobamba. Este proyecto de tesis se enfoca en la cuenca de Guayllabamba. La cuenca de Guayllabamba está constituida principalmente de depósitos volcánicos y volcanoclásticos. Esta cuenca está dividida en dos secuencias: inferior y superior, separadas por una discordancia. Este trabajo se enfoca en la formación San Miguel que pertenece a la secuencia superior. Se estudiará la deformación encontrada en la formación San Miguel. Tres tipos de estructuras de deformación fueron encontradas: estructuras de escape de fluidos, estructuras de acortamiento, y fallas de alto ángulo. Las dos primeras estructuras están correlacionadas con deformación de sedimentos blandos mientras que las fallas de alto ángulo se relacionan a dos episodios de extensión en la cuenca de Guayllabamba. Este trabajo consiste de tres partes: trabajo de campo, fotogrametría de dron, y el análisis de datos. Veinticinco afloramientos a lo largo de la carretera Tabacundo-Guayllabamba (~13km) fueron descritos en detalle mediante la recolección de datos estructurales, dibujos y fotos de los afloramientos. Un modelo 3d, modelo digital del terreno y un modelo de sombras para un afloramiento fueron obtenidos mediante la fotogrametría de drones. Finalmente, la intensidad de la deformación de los afloramientos de la zona de estudio, la correlación de las estructuras de deformación con los eventos de deformación en la cuenca de Guayllabamba, y la dirección de vergencia de las estructuras de acortamiento fueron obtenidas mediante el análisis de datos. Como resultado se crearon un mapa con las capas representativas a lo largo de la zona de estudio, un mapa de la intensidad de la deformación y un mapa del paleo-stress usando las vergencias de las estructuras de acortamiento. Las diferentes direcciones de paleo-estrés fueron relacionados con diferentes eventos de deformación gravitacional. Finalmente, un modelo tectónico-estructural para la evolución de la cuenca de Guayllabamba fue propuesto.

Palabras clave: Cuenca de Guayllabamba, Formación San Miguel, decollement, estructuras de acortamiento.

ABSTRACT

Ecuador is divided into three main Geological provinces: the Western Cordillera, the Cordillera Real, and the Interandean valley. The Interandean Valley hosts sedimentary basins such as the Chota, Guayllabamba, Ambato-Latacunga, Alausí-Riobamba basins. This thesis project focuses on the Guayllabamba basin. The Guayllabamba basin mainly consists of volcanic and volcanoclastic deposits, and it is divided into two sequences, lower and upper, separated by an unconformity. The project focuses on the San Miguel Formation, which belongs to the upper sequence, where we study the deformation found there. Three types of deformation structures were found: water escape structures, shortening structures, and high angle faults. The two first structures were correlated to Soft Sediment Deformation, while the high angle faults to two different collapse episodes of the Guayllabamba basin. This work consists of a geological survey, drone photogrammetry, and data analysis. Twenty-five outcrops along the Tabacundo Guayllabamba road (~13km) were described in detail by collecting structural data, sketches, and pictures of the outcrops in the field. A 3D model, Digital surface model, and hillshade for an outcrop were obtained in the drone photogrammetry part. Finally, the deformation intensity of the outcrops in the study zone, the correlation of the deformation structures with the deformation events in the Guayllabamba basin, and the vergence direction of the shortening structures was obtained in the data analysis part. As result, we created one map for the most representative beds along the Guayllabamba basin, a map for the deformation intensity, and a paleostresses map with the shortening structures vergences. The paleostresses were correlated to different events of tilting. Finally, a structural tectonic model for the evolution of the Guayllabamba basin was proposed.

Key words: Guayllabamba basin, San Miguel formation, decollement, shortening structures.

INDEX

INDEX	i
LIST OF FIGURES AND TABLES.....	iii
1. Introduction	1
1.1. Background information	1
1.2. Study area.....	2
1.3. Objectives.....	3
2. Geologic framework.....	4
2.1. Tectonic Setting.....	4
2.2. Regional Geology.....	5
2.3. Inter-Andean valley	6
2.4. Guayllabamba basin	7
Lithostratigraphic units of the Guayllabamba basin.....	7
2.5. Soft sediment deformation (SSD) and Mass transport deposits (MTDs).....	12
3. Methodology	14
3.1. Geological survey.....	14
3.2. Drone photogrammetry	14
3.3. Data analysis	15
4. Results	16
4.1. Water escape structure	17
4.2. Shortening structures.....	18
4.3. Intensity of the deformation	27
4.4. Vergences direction of the shortening structures	30
4.5. High angle faults and surface expression related faults	34
4.5.1. High angle faults truncated by the unconformity	34
4.5.2. Syn-San Miguel formation fault (Buttress unconformity)	34
4.5.3. High-angle faults that cut Post San Miguel formation units.....	36
4.5.4. Slide scars related to the current Guayllabamba depression	36
4.6. Stereonet analysis.....	37
4.6.3. Fractures	38

5. Discussion	40
6. Conclusion.....	48
7. Recommendations	49
8. Bibliography	50

LIST OF FIGURES AND TABLES

Figure 1	2
Figure 2	4
Figure 3	6
Figure 4	9
Figure 5	13
Figure 6	14
Figure 7	16
Figure 8	17
Figure 9	18
Figure 10	19
Figure 11	20
Figure 12	21
Figure 13	22
Figure 14	23
Figure 15	24
Figure 18	27
Figure 19	28
Figure 20	29
Figure 21	30
Figure 23	32
Figure 24	33
Table 1	34
Figure 26	36
Figure 27	37
Figure 28	39
Figure 29	41
Figure 30	43
Figure 31	44
Figure 32	46

1. Introduction

1.1. Background information

Sedimentary basins are areas where sediment is accumulated and preserved. The preserved sediments provide information about the depositional environment in which they were accumulated and the geologic processes that occurred in the period while the sediments were deposited (Streit et al., 2017). They constitute a record of the erosion and uplift of the surrounding mountain areas (Rodríguez-Fernández & Sanz de Galdeano, 2006; Sobel et al., 2003); in the case of an intermontane basin such as the Guayllabamba basin. In addition, they develop in different tectonic settings. One of these tectonic configurations is convergent settings, such as the one in Ecuador. However, they can also be found in trenches, fore-arcs, intra-arcs, back arcs, and retroarcs (Ingersoll, 2011).

Ecuador hosts several sedimentary basins along the Interandean valley from north to south: Chota, Guayllabamba, Ambato-Latacunga, and Alausí-Ríobamba (Winkler et al., 2005). The focus of our study is the Guayllabamba basin, an intermontane basin that mainly consists of volcanic and volcanoclastic deposits of the Pliocene age, which can be defined by two sequences separated by an unconformity (Villagómez, 2003; Martin-Merino et al., 2021). The first sequence contains the Upper Pisque Formation and the San Miguel formation. The second sequence contains the Guayllabamba, Chiche, Machangara, Mojanda, and Cangahua formations. The San Miguel formation exhibits several phases of deformation (Villagómez, 2003; Martin-Merino et al., 2021), characterized by gravity-induced folding, as well as later high angle faulting.

Deformation occurs mainly due to two factors: tectonic forces or driven by gravity. The evidence of these deformations is preserved in the form of fold and thrust, fractures, and joints. On the other hand, soft-sediment deformation also exists where sedimentary and tectonic processes are recorded before complete lithification and during/after sedimentation (Audemard & Michetti, 2011; Van Loon, 2009). They are driven by tectonics (such as deformation associated to earthquakes) or by gravity (such as olistotromes at tilted margins). They are characterized by clastic dykes, flame structures, convolute lamination, recumbent folds, syn-sedimentary faults, and slumps (Montenat et al., 2007; Van Loon, 2009). In the Guayllabamba basin, the Upper Pisque and San Miguel formations mainly exhibit soft-sediment deformation that is driven by gravity (López & Toro, 2019; Martin et al., 2021; Villagómez, 2003).

The Guayllabamba basin stratigraphy has been previously documented (López & Toro, 2019; Martin et al., n.d.; Pacheco et al., 2014; Villagómez, 2003). The stratigraphy from Upper Pisque and San Miguel Formation has been detailed by López & Toro, (2019) and Martin-Merino et al., (2021)65. However, detailed deformation studies have not been done. The detailed structural characterization of the deformation would provide information about the relation between the soft sediment deformation structures and the syn-sedimentary and post-sedimentary processes (Owen, 1987) that affected the Guayllabamba basin.

1.2. Study area

The study area is located in the Northern part of Ecuador, in the Guayllabamba basin along the Guayllabamba-Tabacundo road. The study area is delimited in a square of approximately 48 km², as shown in Figure 1A.

The detail of the area is shown in Figure 1B. The study starts at the Cochasqui Toll following the Guayllabamba-Tabacundo road and ends one kilometer westward from the Guayllabamba-Cayambe roundabout. A few secondary roads were also studied.

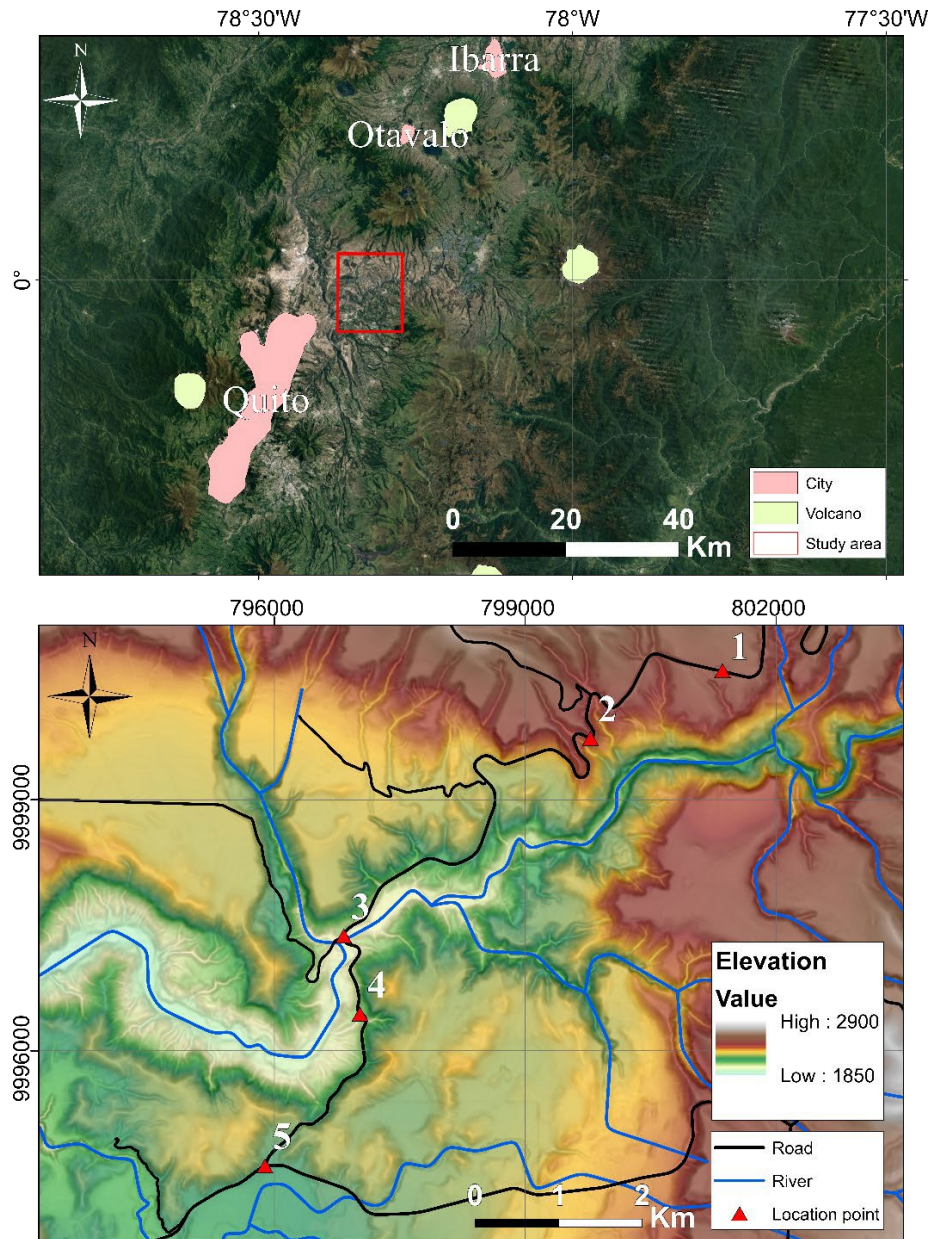


Figure 1.- (A) Satellite image with the study area highlighted in a red square. The main cities and volcanoes near the study area are also shown. (B) Map of slope and elevation (in both cases darker represents a higher value) of the study area showing the main road, secondary roads, rivers and five geographic reference points: 1. Cochasqui Toll, 2. Pisque viewpoint, 3. Pisque river bridge, 4. Pisque adventure park, and 5. Guayllabambaroundabout.

1.3. Objectives

The main objective of this work is to characterize the deformation of the Upper Pisque and San Miguel Formation along the Guayllabamba-Tabacundo road, between the Cochasqui Toll and the Guayllabamba roundabout, which represents a length of ~13 km.

The specific objectives are:

- Create a geologic map along the road establishing the geometry and amount of deformation.
- Take structural measurements and descriptions of the observed structures.
- Create a paleoslope map using the geometry of gravity-driven deformation features.
- Create a model of a representative fold using drone-captured imagery and photogrammetric techniques to characterize its geometry in detail.
- Analyze the structural data to better understand the deformation processes and the geometry of the observed structures and infer paleostresses.

2. Geologic framework

2.1. Tectonic Setting

Ecuador is located at a convergent margin where the Nazca Plate (Figure 2) subducts beneath the South American plate at a rate of 57mm/year - 70mm/year and its convergence azimuth is about N81°E to N120°E (DeMets et al., 1990; Gutscher et al., 1999; Kellogg et al., 1995; Norabuena et al., 1999; Pardo-Casas & Molnar, 1987). Nazca plate was created due to the fragmentation of the Farallon plate at 25 Ma (Gutscher et al., 1999).

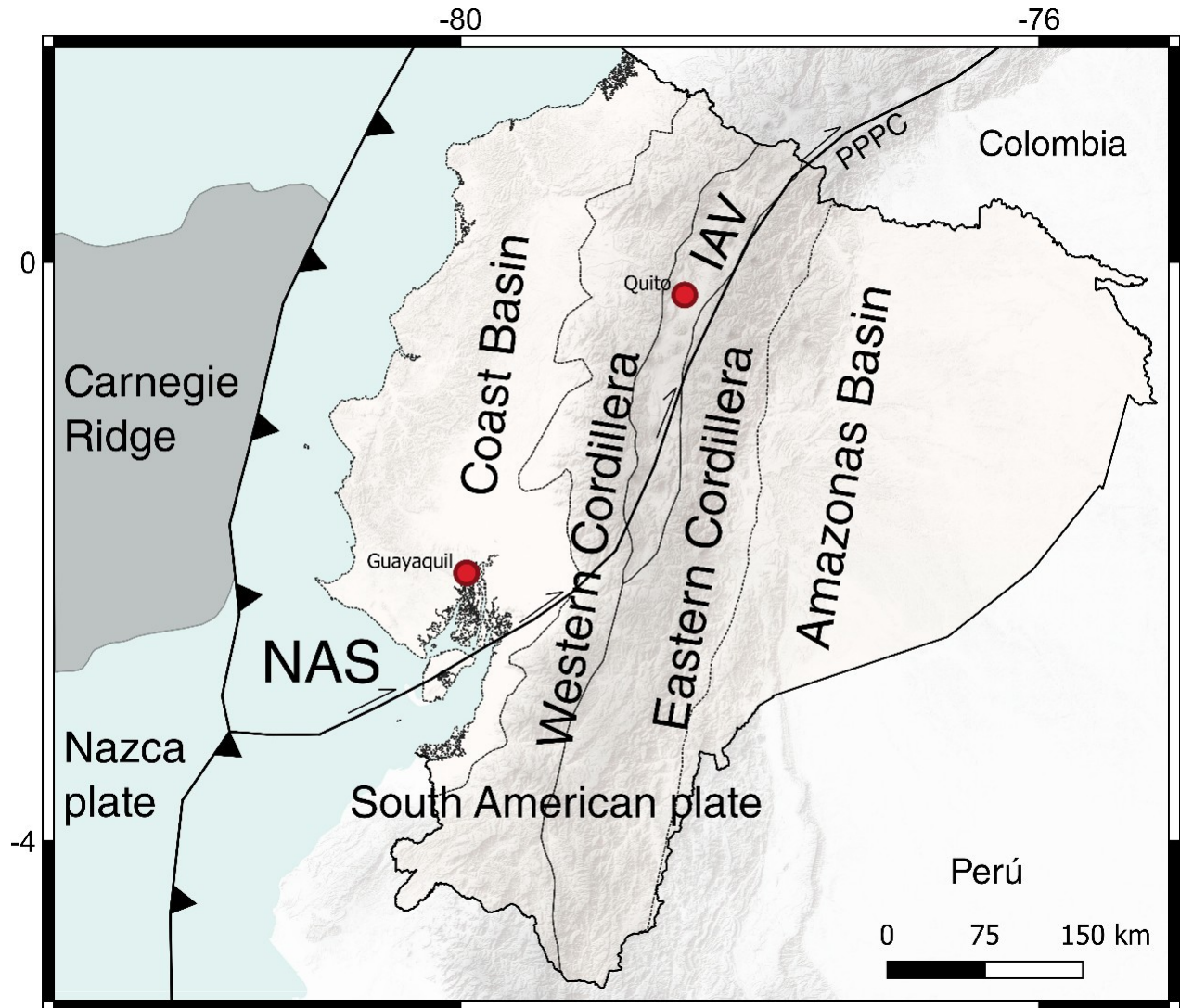


Figure 2.- Main Ecuadorian Geologic provinces: Coast basin, Western Cordillera, IAV (Interandean valley), Eastern Cordillera, and Amazonas basin in the Geologic tectonic context of Ecuador modified from R. A. Spikings et al., (2000) and Vallejo, (2007).

On the other hand, the Carnegie Ridge is obliquely colliding with the South American plate (Figure 2) and is interpreted as created due to the motion of the Nazca plate over the Galápagos hot spot

(Gutscher et al., 1999). This convergence has changed angle and velocity through time (Pardo-Casas & Molnar, 1987).

The interaction between the Nazca plate, South American plate, and Carnegie ridge results in the tectonic stresses in the Puna, Pallatanga Cosanga, and Chingual fault system creating the NAS, as seen in figure 2 (Alvarado et al., 2016). The North Andean Sliver (NAS) migration in an oblique convergence 15 Ma generated a narrowing in the restraining bends zones (Alvarado et al., 2016). The NAS moves east to northeastwards with a velocity of 7.5 – 9.5 mm/year (Nocquet et al., 2014).

2.2.Regional Geology

Continental Ecuador is separated into five main geologic domains from West to East: Coast Basin, Western Cordillera, Inter-Andean valley, Eastern Cordillera, and Amazon basin, as seen in Figure 2.

The Coast Basin is formed by a mafic igneous basement with sediments that span from the Late Cretaceous to the Quaternary, with volcanic sources overlying the basement (Benitez, 1995). The same basement forms the Western Cordilleras and the Coastal Basin, overlain by deep water deposits (Vallejo, 2007). Both provinces originated in the Late Cretaceous by the collision of an oceanic plateau with the South American plate (Hughes & Pilatasig, 2002; Vallejo, 2007).

The Inter Andean Valley (IAV) is a tectonic depression filled by volcanoclastic and sedimentary deposits from Late Miocene-Pliocene (Winkler et al., 2002). The basins along the IAV were formed due to tectonic rearrangements in the Ecuadorian Andes during the Late Miocene – Recent (Winkler et al., 2005). Furthermore, the main Ecuadorian sedimentary basins are located in the northern part of the Interandean Valley: Chota Basin, Quito-San Antonio- Guayllabamba basin, and Ambato-Latacunga basin (Figure 3).

The Cordillera Real (Eastern Cordillera) is made of metamorphic rocks dating from the Early Cretaceous to Paleozoic (Hughes & Pilatasig, 2002; R. Spikings et al., 2021; Vallejo et al., 2009). It is the product of the collision of the South America Plate against the Caribbean Plateau (Vallejo, 2007). It has been subdivided into five regional units separated by important regional faults (Aspden & Litherland, 1992)

The Amazon Basin is a hydrocarbon-rich retro-foreland basin dated Mesozoic to Cenozoic that lies over an older cratonic basement (Hughes & Pilatasig, 2002)

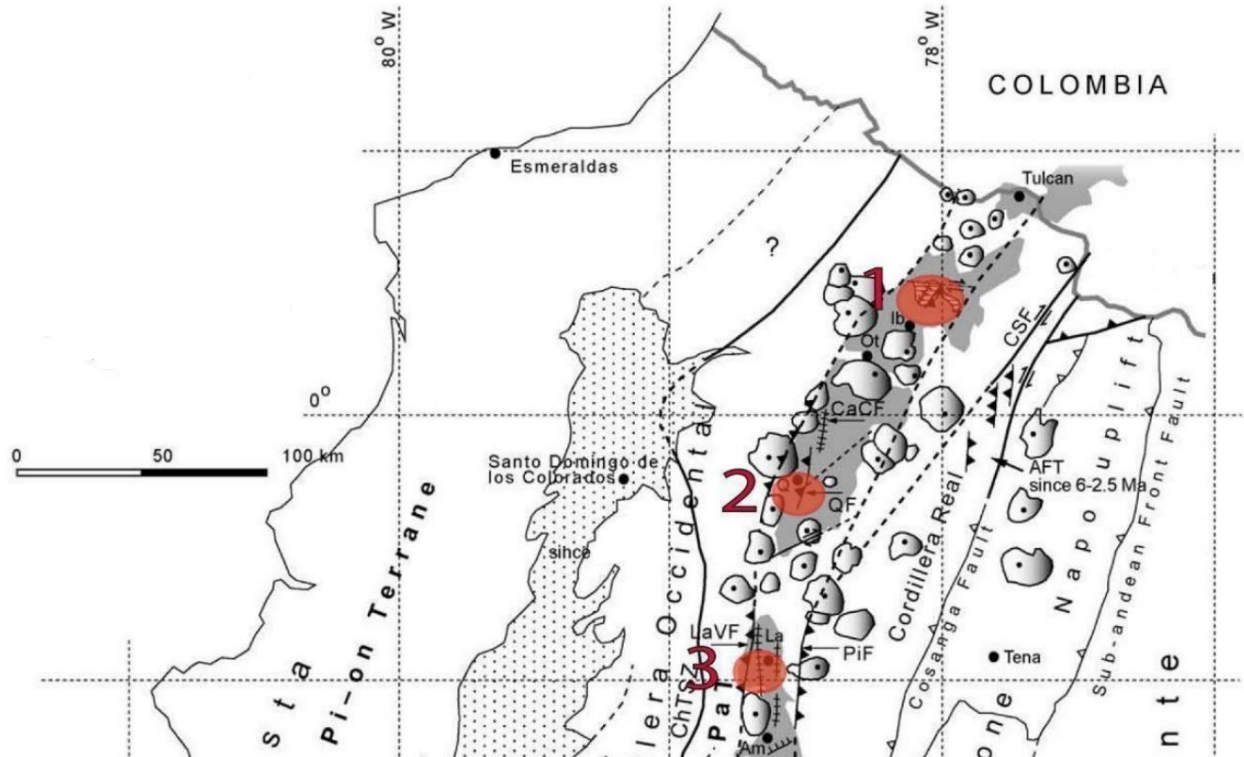


Figure 3.- Basins of the Interandean Valley (IAV) in northern Ecuador: 1. Chota basin, 2. Quito-San Antonio-Guayllabamba basin, 3. Ambato-Latacunga basin. Map taken from Reinoso (2021) and Winkler et al. (2005)

2.3. Inter-Andean valley

The Inter-Andean valley is the region that goes from the Colombian border to about 2°30' (Winkler et al., 2005). It is 300 km long and 20 to 30 km wide. The Peltetec fault (Late Jurassic) is the eastern IAV border. This fault formed due to the accretion of the Eastern Cordillera or the accretion of Pallatanga block in the Late Cretaceous (Litherland, 1994; Winkler et al., 2005). While the suture Calacalí-Pujilí-Pallatanga is western IAV border.

The IAV is separated into three segments due to volcanic complexes. The first segment is Otavalo-Chota, the second segment is Quito-Guayllabamba, and the third segment is Latacunga-Riobamba. Cusín and Mojanda volcanoes separate the first and second segments. The second and third segments are separated by Rumiñahui, Pasochoa, Cotopaxi, and Illiniza volcanoes. (Villagómez, 2003)

There are various proposed models about IAV formation, development, and structures:

- Extensional events that generated a Mio-Pliocene graben (Villagómez, 2003; Winter, 1990).
- The IAV is a transported basin due to low angle thrust (Piggyback) through four tectonic extensive and compressive pulses (Tibaldi & Ferrari, 1992). This is related to the

interaction between Western Cordillera and Eastern Cordillera in the geologic, tectonic Pliocene-Quaternary framework.

- The IAV is a restraining bend, and the Northern Ecuadorian Andes belongs to a transpressive zone with a stress azimuth E-W almost constant in the Early Pleistocene according to shallow focal studies (Ego et al., 1996)
- The IAV has been formed in a compressive zone in a spindle-shaped basin type since 6 Ma. It is a product of the arrival of the Carnegie Ridge to the Ecuadorian trench, where the basin was opened and closed due to increasing and decreasing the convergence rate (R. A. Spikings et al., 2005; Villagómez, 2003)
- The initial stage of the interior IAV basins is the product of extension with a tectonic inversion after 0.78 Ma (Middle Pleistocene), according to Barragán et al. (1996), Villagómez (2003) and Winkler et al. (2002).
- There is a strike-slip behavior in Northwestern South America due to the migration of the North-Andean Sliver because it has internal deformation. This block moves through a fault system in a transpressive environment, and its deformation is shown in the Quito thrust fault and the North-Andean depression (Alvarado et al., 2016)

2.4. Guayllabamba basin

The Guayllabamba basin is mainly composed of volcanic and volcanoclastic deposits (Villagómez, 2003). The lithostratigraphic units filling it have a thickness of about 300 m to over 600 m. Due to syn-sedimentary tectonic processes, the sedimentary infill record unconformities, disconformities, lateral tapering, and onlap geometries (Martin-Merino et al., 2021). The sedimentary succession can be divided into two primary sequences separated by an unconformity, as seen in Figure 4A. The first sequence (lower sequence) forms basal lava flows, tuffs, fluvial, deltaic, and lacustrine deposits dated 3-0.7 Ma (Late Pliocene to Early Pleistocene). They correspond to Basal lava flow, Golden Tuffs, Lower Pisque, Upper Pisque, and San Miguel Formations. Also, they were deposited in an extensional regime, according to (Villagómez, 2003). While, the upper sequence consists of volcanic deposits, lahars, alluvial sediments, hyperpycnal flows and fluvial deposits dated as 0.78 Ma to recent (Villagómez, 2003), that form part of Guayllabamba, Chiche, Machángara, Mojanda y Cangahua Formations (figure 4A).

Lithostratigraphic units of the Guayllabamba basin

Basal Lava Flows

This formation is considered the base of the stratigraphic succession with a thickness observed up to 200 m. It mainly consists of lava and basaltic scoria in the base and autoclastic breccias in the top, where we found an erosional contact with Golden tuffs formation (Villagómez, 2003).

According to (Villagómez, 2003), the lavas consist of plagioclases (labradorite-bytownite), orthopyroxenes (enstatite), and magnetite over a matrix of plagioclase microliths and glass. It is

interpreted as the Pliocene age due to its correlation with near volcanos that have the following ages: Casitagua 2.25 ± 0.5 Ma (OLADE-INECEL, 1980), Cubilche and Chicaloma 2.6 ± 0.06 , and 3.46 ± 0.1 Ma (Barberi et al., 1988).

Golden Tuffs Formation

This formation thickness is about 100 m, and it consists of siltstones intercalated with tuff sandstones in the base (Villagómez, 2003). In contrast, the top exhibits light brown siltstones intercalated with meter-thick beds of channeled sandstones with pumice clasts (Martin-Merino et al., 2021).

Lower Pisque Formation

This formation consists of tabular and lenticular beds of massive and heteromeric muddy sandstones interbedded with channeled conglomerates, and it exhibits a 60 m thickness (Martin-Merino et al., 2021).

Upper Pisque Formation

This formation consists of tabular and lenticular beds of massive, graded, and parallel bedded conglomerates breccias and sandstones, and it exhibits up to 75 m thickness (Villagómez, 2003). Martin-Merino et al., (2021) defined the last 30 m of this formation as unit A. It mainly consists of thick massive, graded, and parallel laminated beds of coarse-grained sandstones and gravelly sandstones. These beds are tens of meter-thick bedsets that dip basinward and form clinothems truncated by thick channeled conglomerates towards the upper part and a fining-upward sequence of sandstone outcrops.

San Miguel Formation

DGGM (1977) initially defined the coarse grain sandstones, tuffs, and tuff-rich siltstones that outcropped 4.5 Km NE of San Miguel del Común as the San Miguel Formation. Then, DGGM (1982) included the deformed sediments of Guayllabamba as part of the San Miguel formation. Later DGGM (1982), Samaniego et al. (1994), and Ego et al. (1996) defined this formation as a lacustrine environment with volcanic input.

Next, Villagómez (2003) divided San Miguel Formation into two members: San Miguel and Lacustrine San Miguel. San Miguel member with an 80 m thickness consists of lithic grey-greenish sandstones medium to coarse grain meters to centimeters layers, intercalated with tuff-rich siltstones, tuffs, and reworked tuffs (Villagómez, 2003). Increasing sandstone layers towards the top of the sequence, these sandstones exhibit oxide nodules, and their clasts are andesitic and pumiceous material (Villagómez, 2003). Lacustrine San Miguel member with a thickness of 80 m to 200 m, in the lower sequences where deformation is not exhibited consists of centimeters interbedded tuff-rich siltstones, white-beige claystone (bentonite type), and dark fine sandstones. While in the upper sequences (deformed), claystone, siltstones, and tuff are found with light colors,

white to beige, where deformation and meters to centimeters slump are exposed (Villagómez, 2003).

A new detailed stratigraphic classification was made by Martin-Merino et al. (2021). The San Miguel Formation (Figure 4B) was divided into units B, C, and D. Unit A is not part of the San Miguel formation but part of the Upper Pisque Formation. A Fe-oxidized crust is between units B and C.

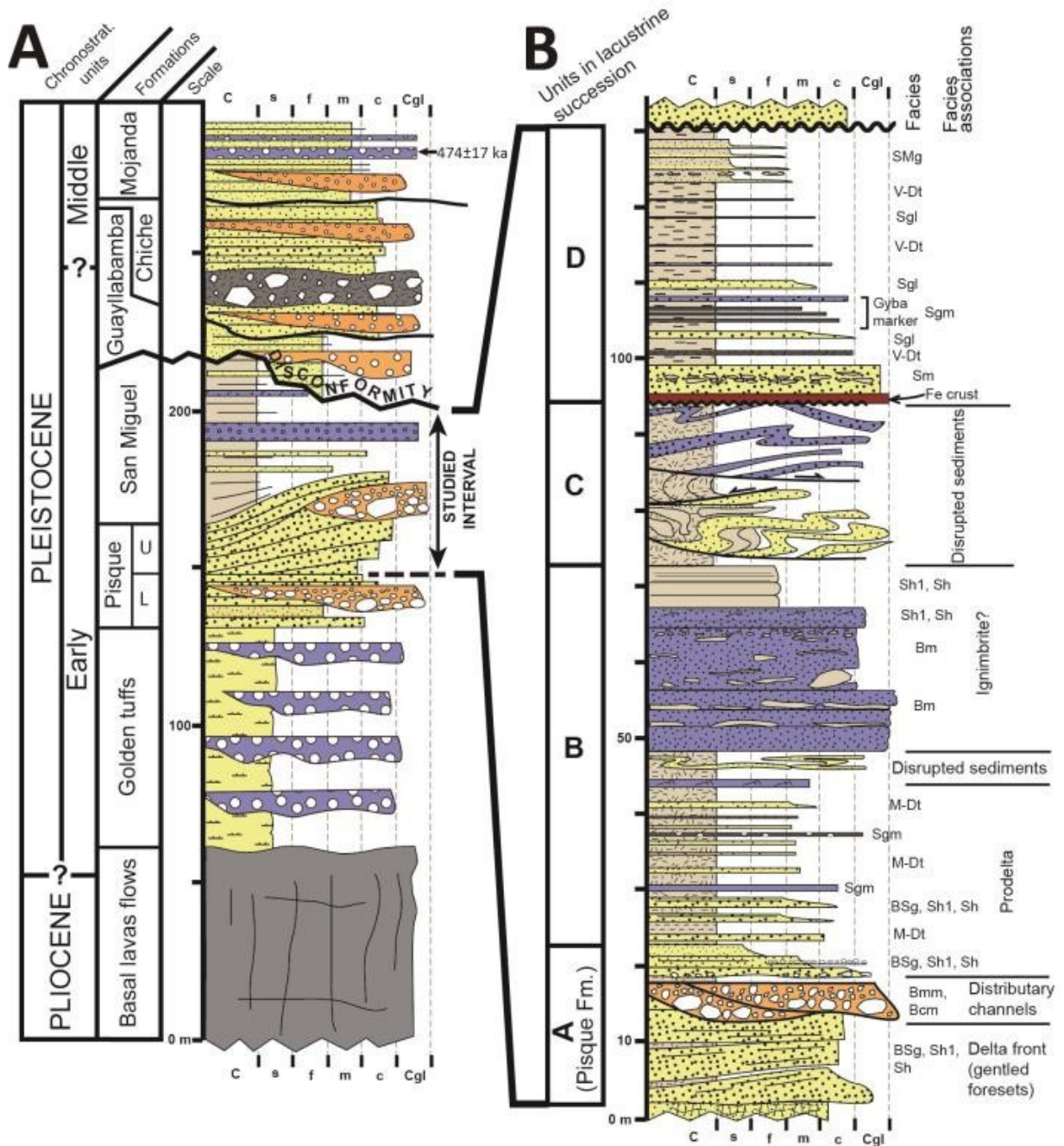


Figure 4.- (A) Guayllabamba basin stratigraphic column (B) San Miguel Formation stratigraphic column taken from Martin-Merino et al. (2021).

Unit B

This unit is approximately 55 m thick, and it consists of massive diatomites interbedded with tabular centimeters to meter-thick very coarse sandstones and volcanic tuffs. Chaotic deposits form with folded and disrupted sandy beds approximately 2 meters thick towards the upper part. In the top, a 20 m thick sand to gravel-sized clast supported pumice-rich layer is outcropping (Martin-Merino et al., 2021).

Unit C

This unit has a maximum thickness of approximately 50 m, and it consists of highly disrupted gravity flow deposits where slump and faulted beds are exhibited. It is interpreted as syn-sedimentary deformation. In the middle part, a lava body of andesitic composition of up to 15 m thickness is outcropping. Finally, the Fe-Oxidized crust of up to ten cm-thick divides unit C from unit D (Martin-Merino et al., 2021).

Unit D

This unit is after Fe-oxidized crust. It has a thickness of up to 40 m, and the main feature that the unit exhibits is well-developed varved diatomites. A ~5 m layer of laminated, massive, and graded sandy beds intercalates the diatomites layer. There is a series of tabular, massive layers of scoria, ash, and then a layer of pumice and crystals referred to as the GYBA marker (Figure 4B), that outcrops towards the top of unit D and serves as a regional marker throughout the basin (Martin-Merino et al., 2021).

Guayllabamba Formation

The Guayllabamba Formation represents a period of intense volcanism and tectonic activity (Martin-Merino et al., 2021). The ages indicate to be Pleistocene according to (OLADE-INECEL, 1980) K/Ar andesite, 1.62 ± 0.16 Ma, and K/Ar rhyolite, 0.98 ± 0.13 Ma (Barberi et al., 1988). Villagómez (2003) proposed subdividing it into four members: Lahar, Domo, Volcanic, and Alluvial.

Lahar member I

It consists of meter mudstone flow with claystone and sandstone clasts. It also has volcanic and pumiceous clasts in a muddy matrix. The thickness varies from 30 m to 60 m in the current Guayllabamba depression and up to 100 m via Oyacoto. Catequilla and Pacpo domes and the Ruco Pichincha can be the source due to the acid composition of the clasts (Villagómez, 2003).

Domo member

It consists of two types of geochemical compositions: acids, subintrusive quartzdiorite, and rhyolite, intermediate with black andesitic xenoliths, and they were considered part of Pacpo and Catequilla domes (Villagómez, 2003).

Volcanic member

It consists of lava flows, debris, blocks, ash, and altered lavas. According to Villagómez (2003), they come from Pichincha and Ilaló volcanic complex. They have correlated with (OLADE-INECEL, 1980) K/Ar andesite, 1.62 ± 0.16 Ma, and K/Ar rhyolite, 0.98 ± 0.13 Ma (Barberi et al., 1988).

Alluvial member

It consists of alluvial sequences with andesitic meter blocks in an inverse graded sandstone matrix (Villagómez, 2003).

Chiche Formation

It consists of conglomerates, coarse sandstones, and tuffs. It has been subdivided into four members (Samaniego et al., 1994). It exhibits channel and floodplain deposits of sand-silt grain size (Winkler et al., 2005).

Fluvial-Lacustrine I Member

According to Villagómez (2003), it has a thickness of 10-15 m and consists of beige siltstone and white tuffs interbedded with grey sandstone. Microconglomerates with andesitic lithics and pumice appear in the base. Fine cross-stratified sandstones appear towards the top. It also exhibits oxidated nodules what it is suggesting an oxidation environment.

Lahar Member II

It has a 10 m to 40 m and consists of mudstone flows and hyperpycnal flows. It looks as massive white non-stratified from far away. It shows subangular to subrounded volcanic clasts and sedimentary clasts in a muddy matrix (Villagómez, 2003).

Fluvial-Lacustrine II Member

It has a thickness that varies from 15 to 80 m and consists of tuff-rich siltstones, diatomites, and grey sandstones. The sandstones exhibit cross-stratification, tuff white pumiceous-rich towards Oyacoto (Villagómez, 2003).

Chiche s.s. Member

According to Villagómez (2003), it mainly consists of conglomerates and coarse sandstones interbedded with tuff layers. The conglomerate clasts are andesitic olivine-pyroxene, rhyolitic, and obsidian. It is considered a hyperpycnal flow, and they turn into riverine towards the North. The facies become finer toward the top. Lavenu et al. (1996) found fossil teeth *Glossotherium*. Hence, the middle Pleistocene age (-0.5 Ma) is interpreted for this layer.

Mojanda Formation

It consists of volcanic and volcanoclastic deposits as the product of the Mojanda volcanic complex. The Mojanda formation exhibits lahars and debris flow intercalated with ashes, pyroclastic surges, fluvial sandstones, and conglomerates. The lahars are rich in dark andesitic lithics and scoria, while the debris flow shows andesitic and dacitic blocks (Villagómez, 2003). Finally, the ashes vary in composition from rhyolite to andesite. It also is distinguished due to two layers of white pumice (Robin et al., 1997).

It is middle-late Pleistocene by dating the basal lavas of Mojanda volcanic complex: 0.59 ± 0.06 Ma and 0.5 ± 0.06 Ma, K/Ar whole-rock andesite (Barberi et al., 1988).

Cangahua

It consists of altered yellowish to brownish tuffs interbedded with ashfall, pumice, paleosoils, mudflows, and alluvial channels. It has a thickness from 20 to 50 m (Villagómez, 2003).

2.5. Soft sediment deformation (SSD) and Mass transport deposits (MTDs)

The stratigraphic units of the San Miguel formation exhibit soft sediment deformation (SSD) in specific stratigraphic intervals from the study zone of the Guayllabamba basin (Figure 4). In the context of SSD, concepts such as mass transport deposits, gravity-driven slumps, and overstep thrust sequences are needed.

2.5.1. Soft sediment deformation (SSD)

Soft sediment deformation (SSD) occurs close to the surface in unconsolidated sediments, and it usually occurs rapidly before deposition and during diagenesis (Owen & Moretti, 2011). It requires three conditions: a driving force, a deformation mechanism, and a trigger such as a temporary state change from solid-like to liquid-like (Owen & Moretti, 2011).

The driving forces that generate soft-sediment deformation are gravity acting on a slope, unequal loading caused by topography irregularities in the sediment-water interface, gravitational instabilities due to denser sediments overlying less dense sediments, and shear by currents (Owen & Moretti, 2011). While the deformation mechanism consists of stresses that exceed the normal sediment strength (Maltman, 1987). Finally, the triggers are the start of deformation mechanisms. Some triggers are earthquakes, waves, floods, rapid sedimentation, and groundwater movements (Owen & Moretti, 2011).

2.5.2. Mass Transport deposits

Mass transport deposits are characterized by chaotic disruption and amalgamation of strata on the seafloor and mountain ranges (Weimer & Shipp, 2004). They are called mélanges or olistostromes, and usually, their sizes are similar to the most significant modern submarine landslides (Camerlenghi & Pini, 2009).

2.5.2.1. Gravity-driven slumps

Gravity-driven slumps are related to slope failure. They initiate at a single point, spread downslope in a compressive regime, and propagate slope in an extensional regime (Farrell, 1984). Then, the displacement of the slump results in compressional folds and thrust at the downslope toe of the basin (Figure 5A). On the other hand, the head is characterized by normal faults. Next, the created extensional faults cut the sediment and create another slope failure (Alsop & Marco, 2013).

2.5.2.2. Overstep thrust sequences

A thrust sequence is considered an overstep thrust sequence if the new thrusts develop in the hanging wall of older thrusts (Figure 5B). Furthermore, higher thrusts are the youngest displacement, and the lower thrust represents the older displacement (Alsop et al., 2018).

On the other hand, the basal detachment progressively gets inactive as the migration upslope away from the depocentre of the basin. In addition, older thrust keeps a fixed position on the slope. Hence, the thrust system propagates opposite to the transport direction (Alsop et al., 2018).

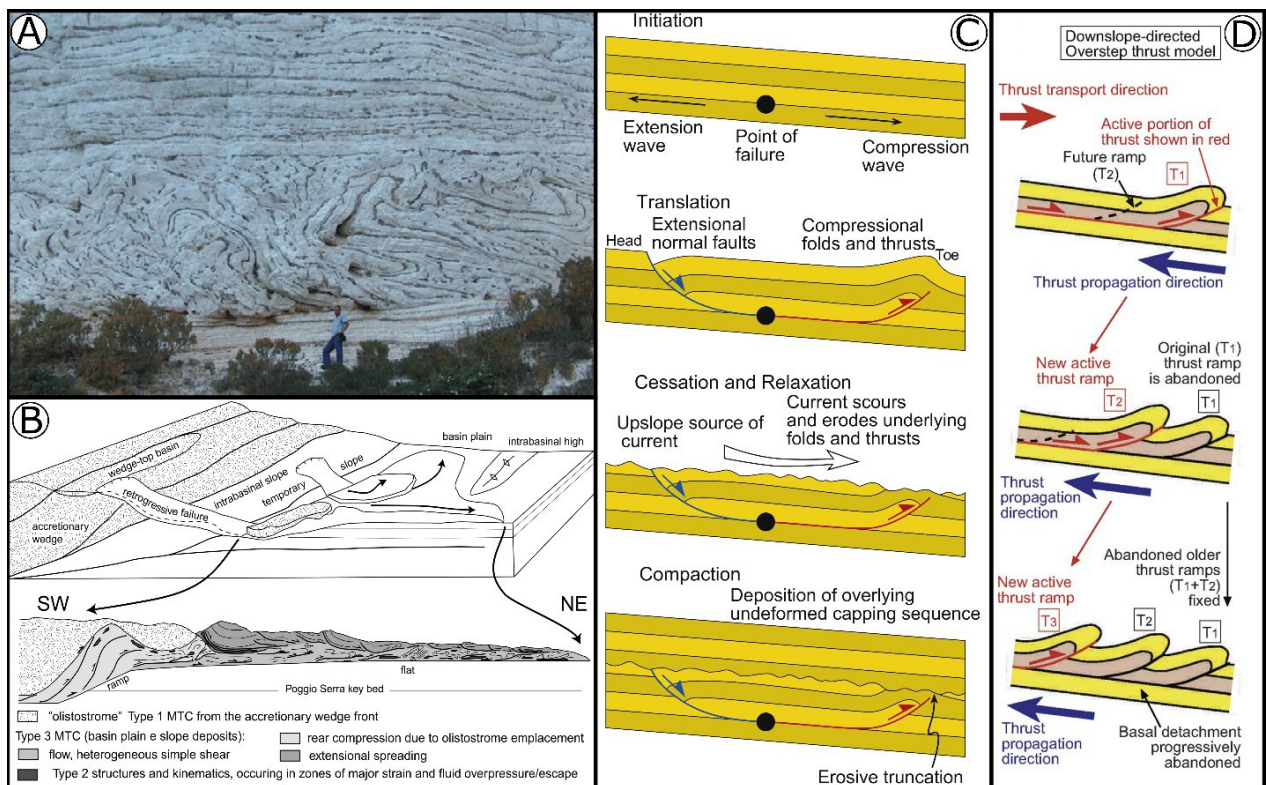


Figure 5.- (A) Soft Sediment deformation example taken from Owen & Moretti (2011). (B) Mass Transport Deposit model taken from Pini et al. (2011). (C) Gravity-driven slump model taken from Alsop & Marco (2013) (D) Overstep thrust sequence model taken from Alsop et al. (2018).

3. Methodology

The work consists of three steps: geological surveys, drone photogrammetry, and data analysis. The geological survey consisted of creating a map with a scale of 1:45000 of the study zone. Then, we highly-detailed described twenty-five outcrops measuring structural data, creating sketches, and taking pictures of the outcrops. Furthermore, a representative outcrop of the study zone where we observe a big fold near the Pisque viewpoint was photographed with a drone belonging to Yachay Tech University. Then, a 3d model was created to help the interpretation of the fold geometry. Finally, the data gathered in the field and the drone was analyzed.

3.1. Geological survey

The geological survey starts with creating a 1:45000 map of the study zone from a 3m resolution Digital Elevation Model (DEM), as shown in figure 1B. Also, four maps of 1:30000 were created to record the information from the outcrops in detail. The map contour lines are every 20 m. Then, 30 cm/pixel resolution orthophotos were used to identify the San Miguel formation outcrops.

Then, twenty-five outcrops were described in great detail. Structural data, sketches, and pictures of each outcrop are included in the descriptions. Attitude data were recorded for bedding planes, fold limb axes, hinge lines, faults, slickenlines, and joints. The azimuth of the outcrop and detailed drawings of the faults, folds, and bedding planes are included in the detailed sketches.

3.2. Drone photogrammetry

Three hundred ninety-six images were calibrated, and about 36487 matches per calibrated image. On the other hand, no 3D ground control points were used. The image capturing positions are shown in Figure 6b. Then, it was processed by an Intel Xeon 3.90 GHz with a ram of 32 Gb and a graphic card NVIDIA T1000 in the Pix4D software. Finally, a 4.62 cm/pixel digital surface model (DSM), 4.62 cm/pixel orthomosaic pictures, cloud points, and a hillshade model were obtained for the outcrop.

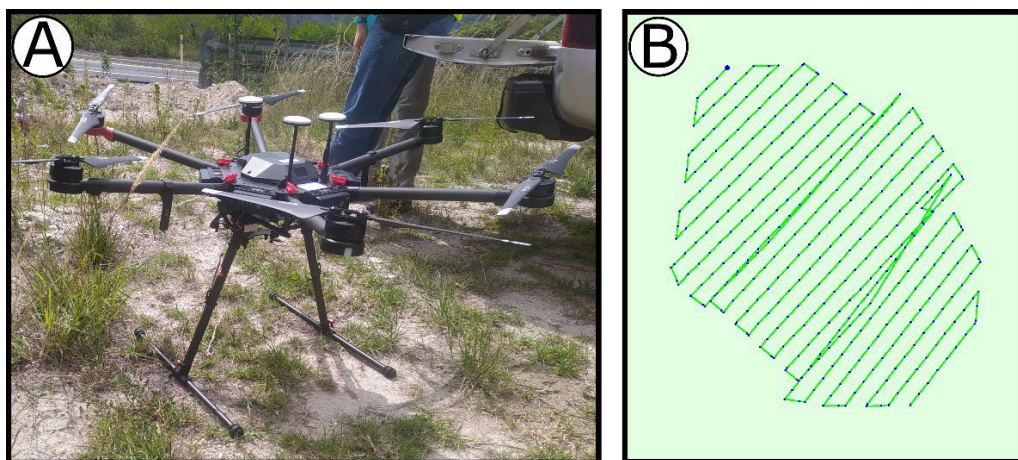


Figure 6.- (A) DJI – Matrice 600 Pro drone belonging to Yachay Tech University. (B) The area captured by the drone.

A representative fold along the Tabacundo-Guayllabamba road between the Pisque viewpoint and the Tanda enter was photographed using a Zenmuse X5R camera installed on a DJI – Matrice 600 Pro drone (Figure 6A) belonging to Yachay Tech University. The photographs have a front overlap of 75% and a side overlap of 65%. The drone flew at 120 m from the floor and mapped an area of 49 ha. In addition, the fly was guided by the program DJI Pilot.

The obtained products were used to study the geometry of the whole outcrop, which cannot be reached due to its height. The products were used to map a syn-sedimentary fault connected to the two sides of the 3D model and understand the cross-cutting relationship in this part of the basin.

3.3. Data analysis

This part of the work consisted in understanding the data gathered in the field and the drone. First, the outcrops were classified according to their deformation intensity. Three intensity levels were created: undeformed, low intensity, and high intensity. Undeformed beds mean low dip bed angles and normal faulting. Low-intensity deformation means low angle dip beds, thrust, and fold deformation. Finally, High-intensity deformation means medium steeply dipping beds to high steeply dipping beds, normal faulting, synforms, and antiforms.

Next, the main structural features include clastic dykes, decollement level, faults truncated by the unconformity, faults that cut post-San Miguel units, and syn-sedimentary faults (Buttress unconformity), and complex folding were related to a stratigraphic level. The stratigraphic levels stated were below Fe crust, below GYBA marker, and above GYBA marker.

Then, the bedding planes, fractures, and faults were analyzed. A map with the bedding planes and the most representative bedding planes was done. The beds' trends were obtained through stereonet statistical analysis. Furthermore, the main fracture trends were plotted in stereonet. Finally, the trend of the primary faults was plotted in stereonet.

In addition, the vergence of some outcrops could be obtained. These outcrops' vergence was obtained by analyzing the thrust transport direction, recumbent folds displacement direction, and slump transport direction. Finally, a map of the vergences of these outcrops was done.

Finally, the drone fly study zone was studied. The DSM was used to create a 3D model of this zone. The hillshade was helpful in connecting the normal fault from both sides of the study zone. In addition, the faults, the recumbent folds, and the sliding planes were described in this zone.

4. Results

In the following chapter, we will summarize the results of our observations in the Guayllabamba basin study zone. Twenty-five outcrops were studied along the Tabacundo-Guayllabamba road (Figure 7), where most San Miguel Formation is outcropping. The outcrops (Figure 7) used the following notation: GBx, where the x varies from 1 to 25. In these outcrops, we observed features such as water-escape structures, shortening structures, and high angle faults.

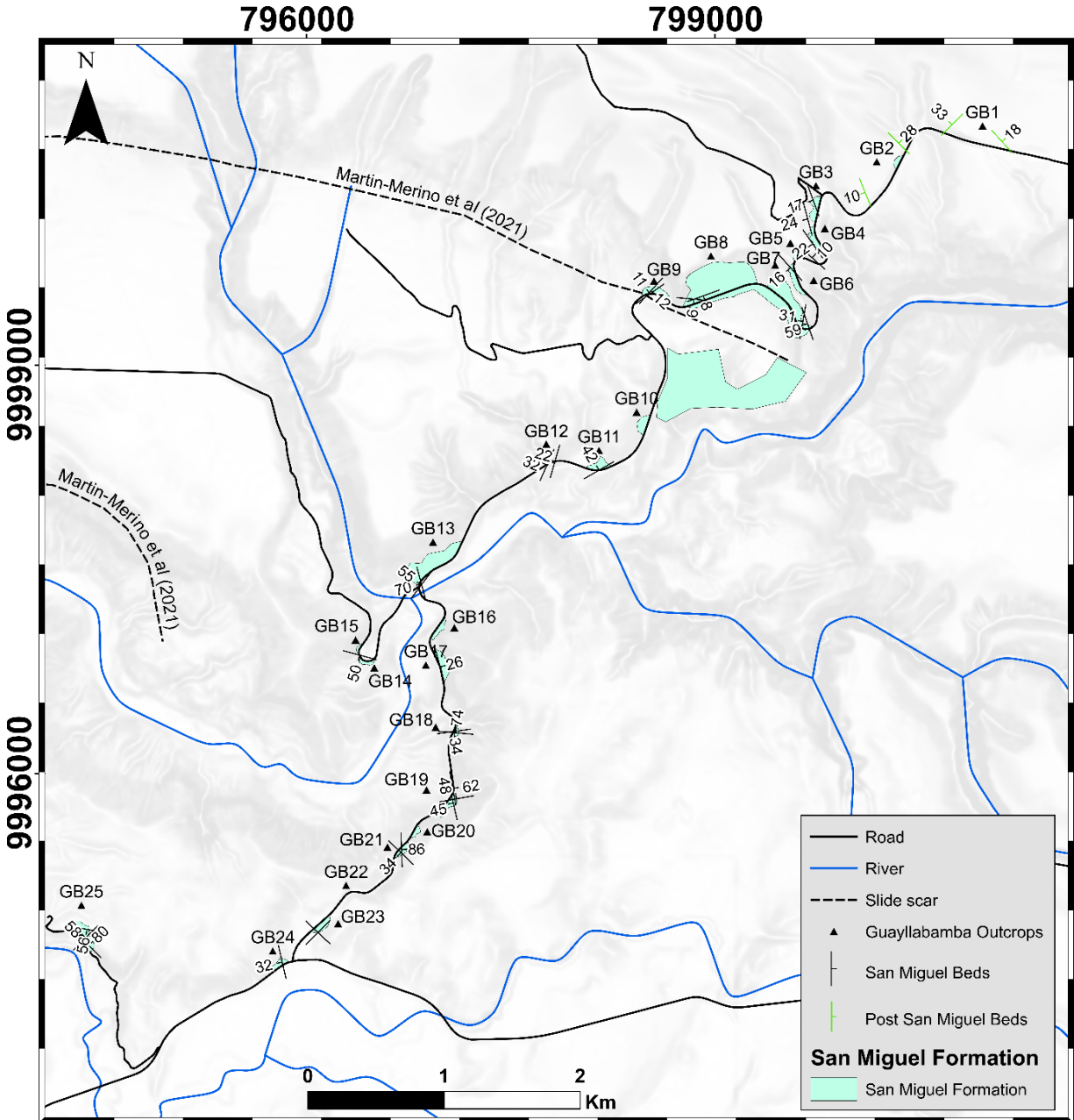


Figure 7.- Map of the most representative bedding planes along the Cochascu Toll-Guayllabamba roundabout road. San Miguel formation outcrops are shown in light blue polygons, while the code corresponding to the outcrops is shown near them above the black triangle. The polygons without code were acquired through the use of orthophotos and binoculars in the field.

The water escape structures seen are a system of sand dykes and sills. The shortening structures observed were thrust and reverse faults, faults related to folds, hanging wall anticlines, footwall synclines, recumbent folds, and overturned antiforms. They are restricted to specific stratigraphic intervals, so they were considered soft-sediment deformation. We also measured the vergence of the shortening structures.

The high angle faults can be divided into faults truncated by the unconformity and those that cut through the unconformity. The latter can be correlated with landslides in the Guayallabamba basin. The faults can be divided into normal faults and likely strike-slip faults. Due to the absence of measured slickensides on the outcrops, we are not sure about the strike-slip kinematics. However, based on Andersonian assumptions, the steeper faults were considered strike-slip faults.

4.1. Water escape structure

The water escape structure observed in the field is a system of sand dykes and sills (Figure 8) which is only found in the outcrop GB8. It is observed below the Fe crust, and it cuts through the ignimbrite and the claystone layers that separate units B to C. The disrupted sediment from unit C restricts it. The geometry and character of these clastic dykes were not studied in detail.

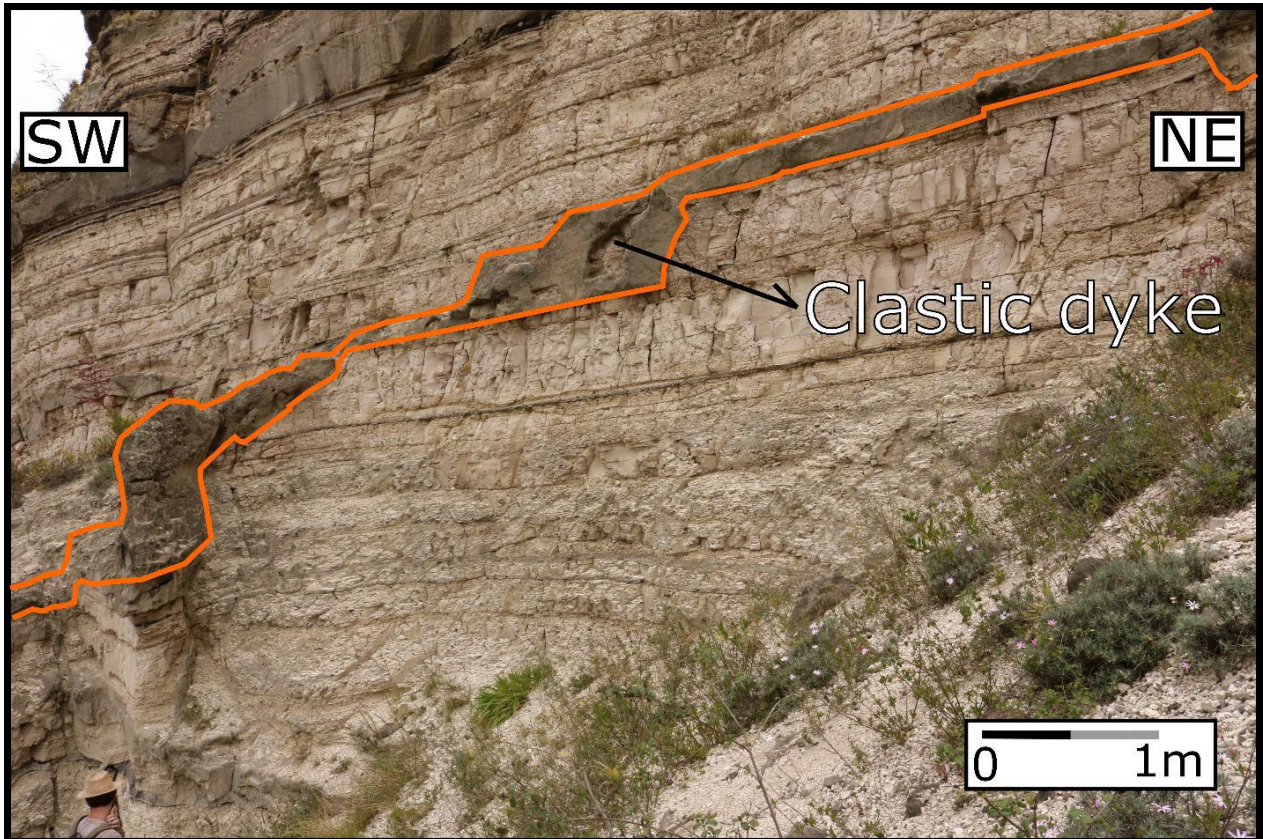


Figure 8.- Outcrop SW-NE of the section GB8 showing the clastic (sand) dyke and sills. See location in Figure 7.

4.2. Shortening structures

The shortening structures were observed in two stratigraphic intervals: below and above the GYBA marker (Figure 4). The shortening structures are older than the high angle faults due to the high angle faults cutting through the shortening structures.

4.2.1. Below GYBA

We observed that the first layers below the GYBA marker were undeformed in the northeastern part of the study zone outcrop GB4 (Figure 7). In contrast, the same layers are deformed in the southwestern part of the study zone in the outcrops GB13 and GB25 (see location in Figure 7), where we observed shortening structures. Hence, the base of the deformation starts after GYBA in the northeastern while it starts before GYBA in the southwestern of the study zone.

The undeformed layers below the GYBA marker from GB4 are shown in Figure 9. We also observed that thrusts deform the layers after the GYBA marker in the same figure. Here is found a decollement level. However, the decollement granulometry was not identified because this part of the outcrop cannot be reached.

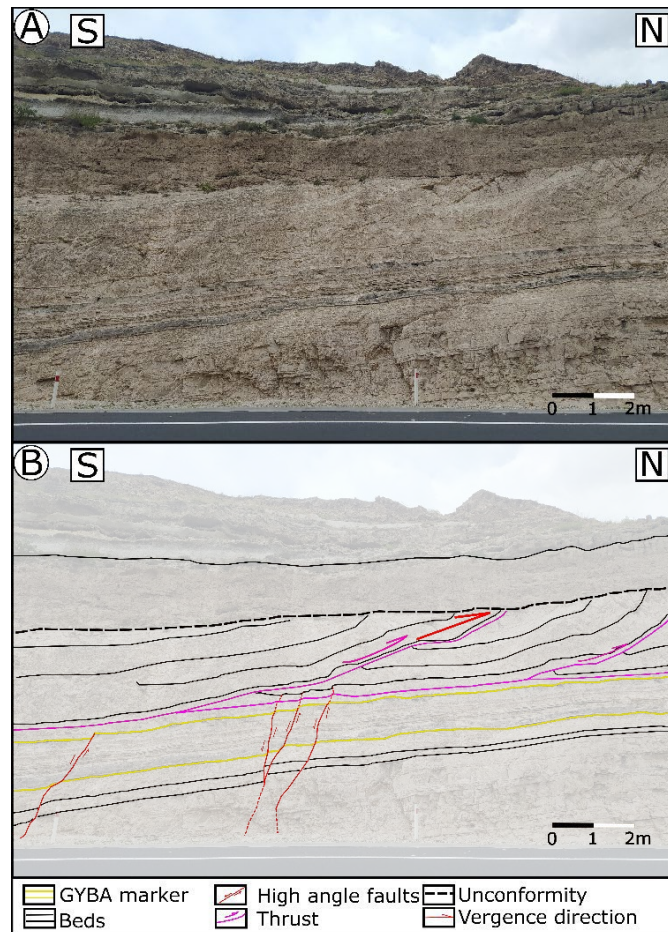


Figure 9.- (A) Outcrop S-N of the section GB4 where we observed layers below GYBA undeformed. The deformation base starts above GYBA marker (B) Interpretation of the section GB4.

On the other hand, the shortening structures from GB13 are shown in Figure 10. We observed antiforms and synforms where one of these folds has a spiral shape. Then, we observed thrusts in opposite directions: towards the NE and SW.

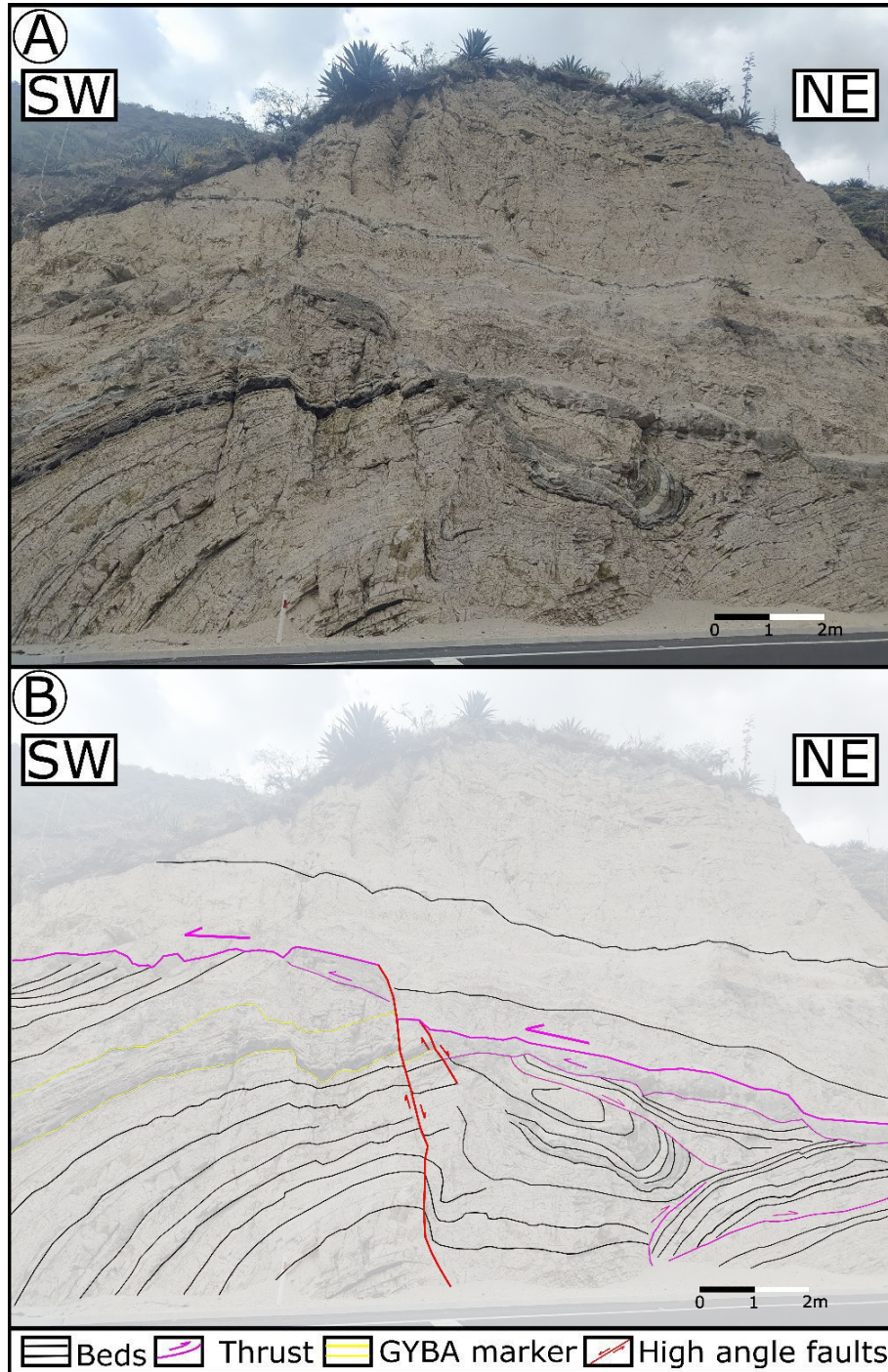


Figure 10.- (A) Outcrop SW-NE of the section GB13 where we observed GYBA marker deformed and shortening structures such as antiforms, synforms, and thrust below GYBA marker (B) Interpretation of the section G13.

Furthermore, the shortening structures observed from GB25 are antiforms, synforms, and thrust faults (Figure 11). We also observed some minor faults correlated with the thrust faults. In this figure, we do not observe the GYBA marker, but GYBA is seen towards the northwest in another part of this outcrop. GYBA was interpreted above the layers seen in Figure 11.

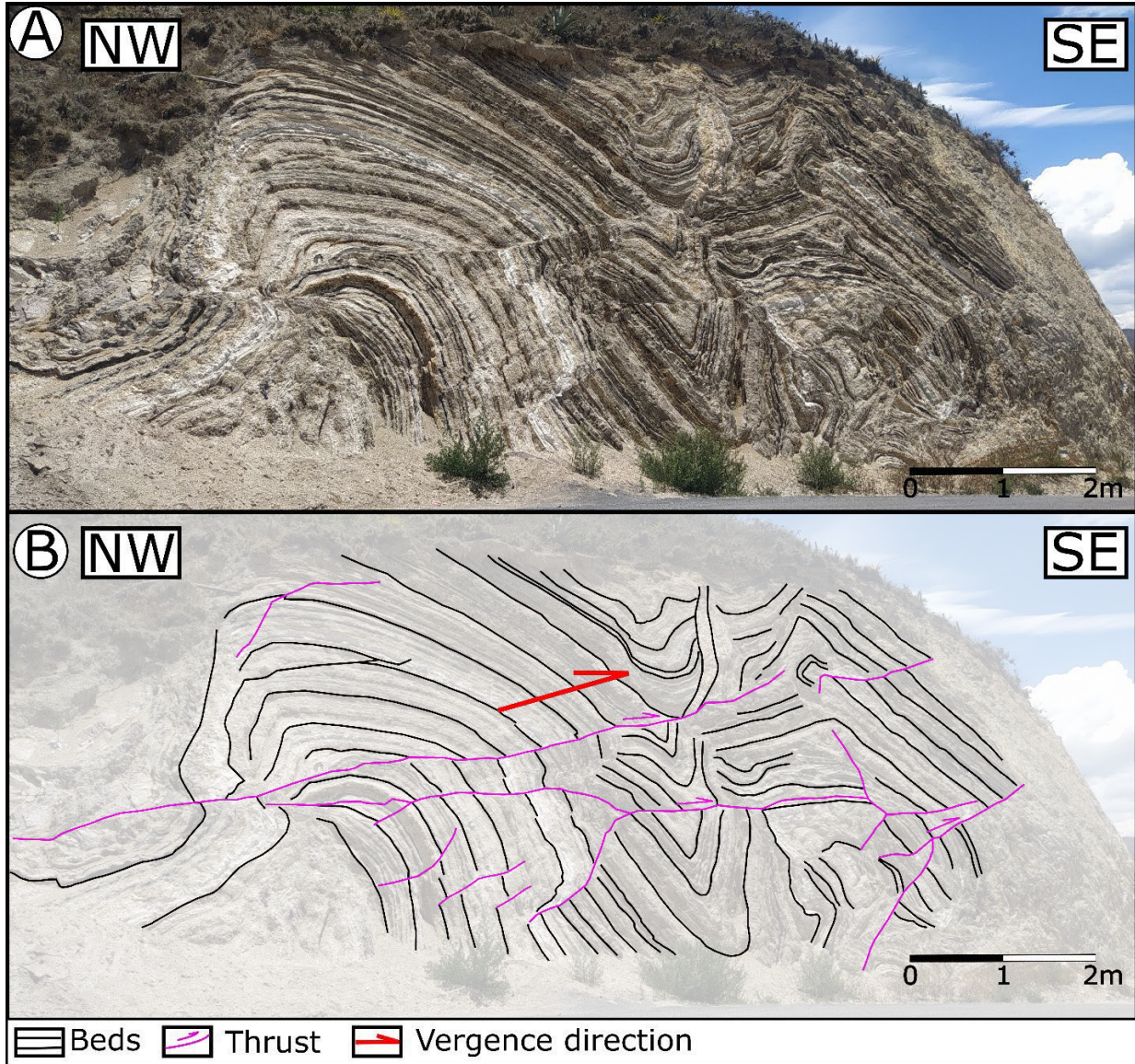


Figure 11.- (A) Outcrop NW-SE of the section GB25 where we observed antiforms, synforms, and thrust. Some faults were unidentified in their kinematic due to the difficulty of finding piercing points. (B) Interpretation of the section GB25.

4.2.2. Above GYBA

We observed thrust faults, footwall syncline, hanging wall anticline, and thrust fault ramps that sole to a decollement level at a centimetric greenish dark ash layer (Figure 12). In addition, there are four white greyish mudstone layers (Figure 13) that are seen in the outcrops GB5, GB6, and

GB7. These beds will be used in this chapter as a marker for the deformation above the GYBA marker.

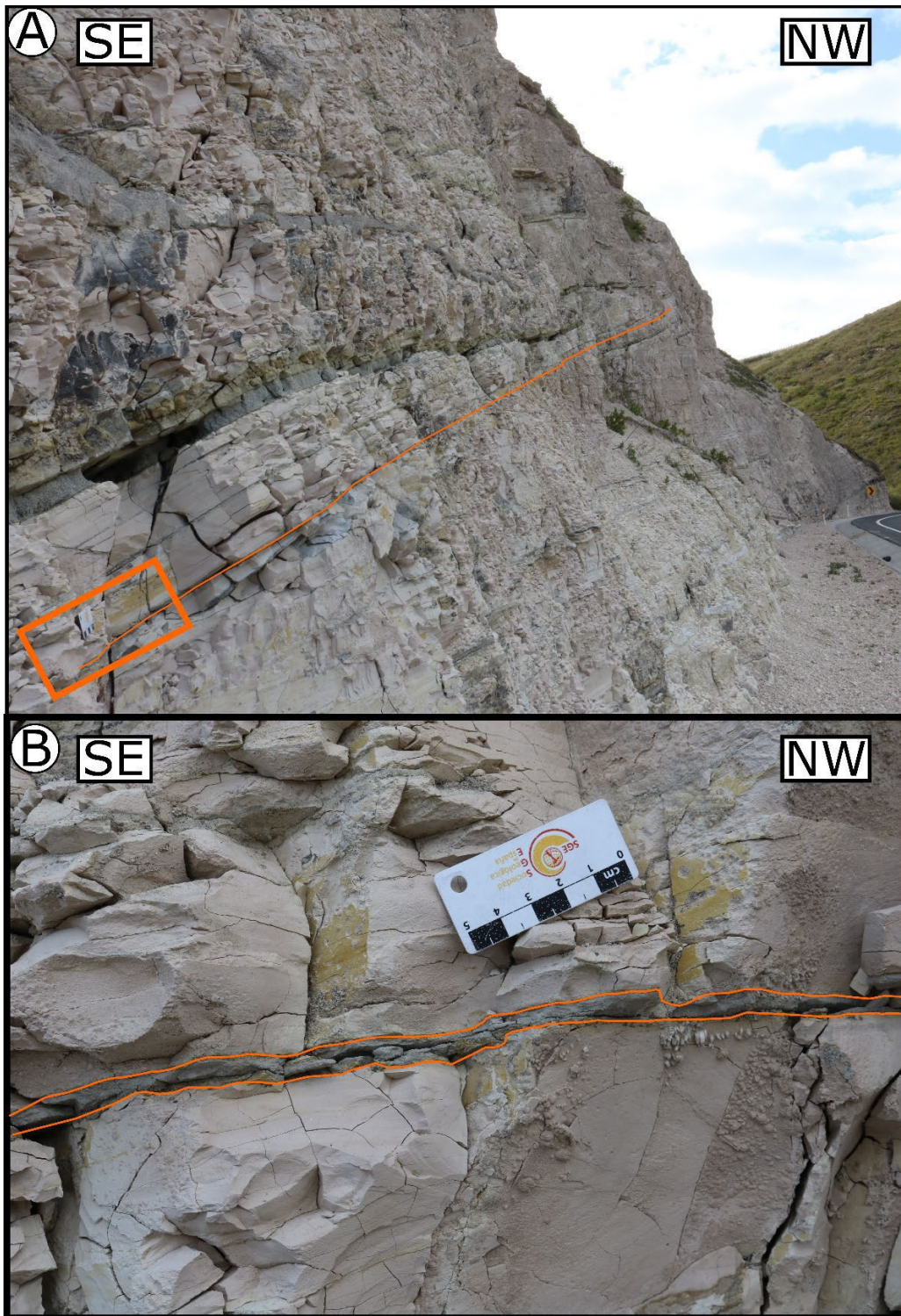


Figure 12.- (A) Section of the SE-NW Outcrop GB6 where we found the greenish dark ash layer that soles the decollement, with a red box showing the zoom of this bed (B) Detailed view from the centimetric greenish dark ash layer

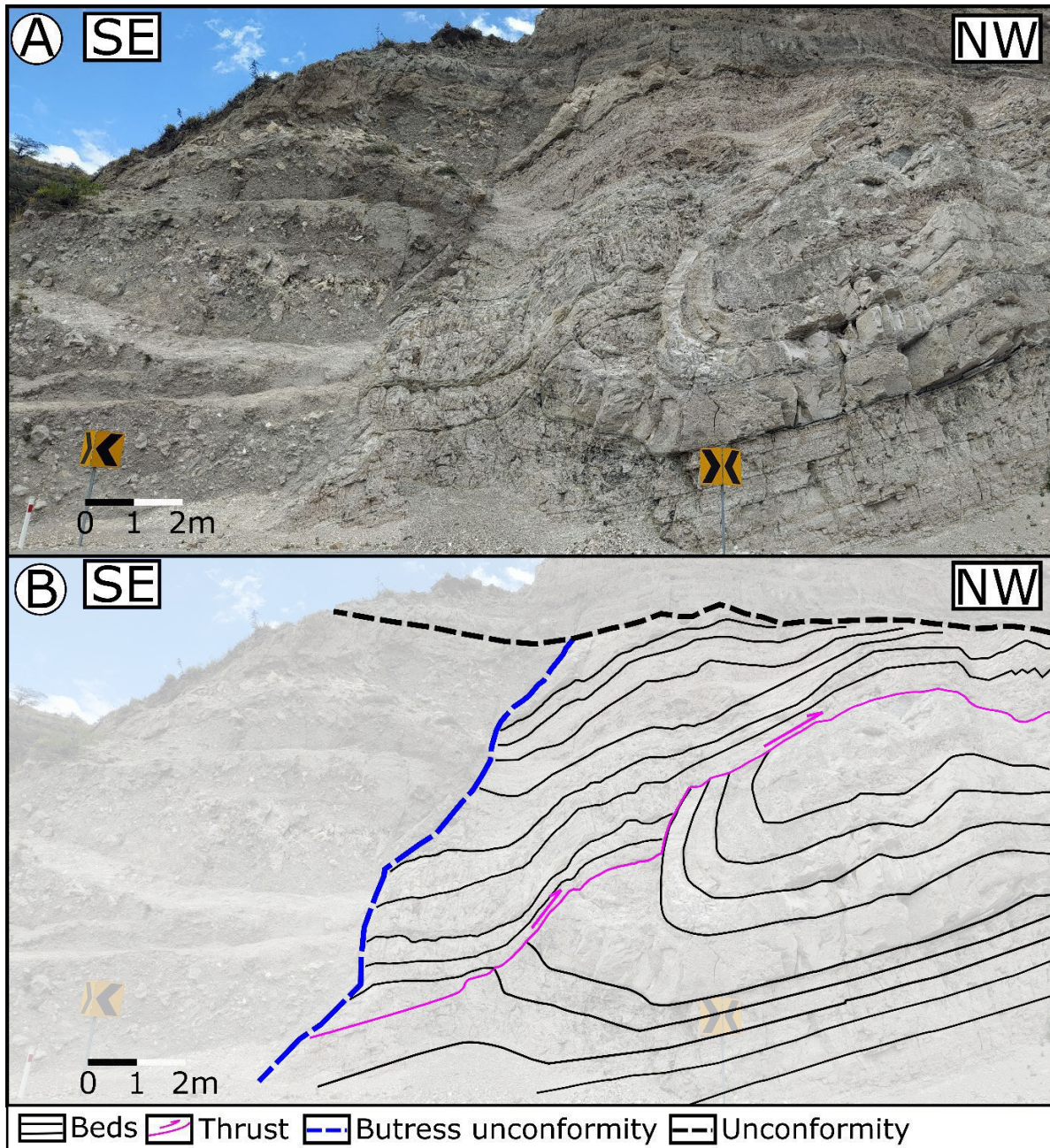


Figure 13.- (A) Section of the SE-NW Outcrop GB6 where we found the four white greyish mudstone layers. (B) Interpretation of the section.

The outcrop GB5 exhibits the four white greyish mudstone layers overturned due to a thrust, as shown in Figure 14. We also observe layers that are not deformed, two faults with unidentified kinematics towards the west, high-angle faults that cut through the folded layers and a talus that is unconformably deposited towards the East of the section GB5 (Figure 14).

In addition, the outcrop GB6 exhibit the four-fault ramps, the decollement level at the centimetric greenish dark ash layer, and the hanging wall syncline (Figure 15). We assume the decollement level is the same as in Figure 9 because both start immediately after GYBA.

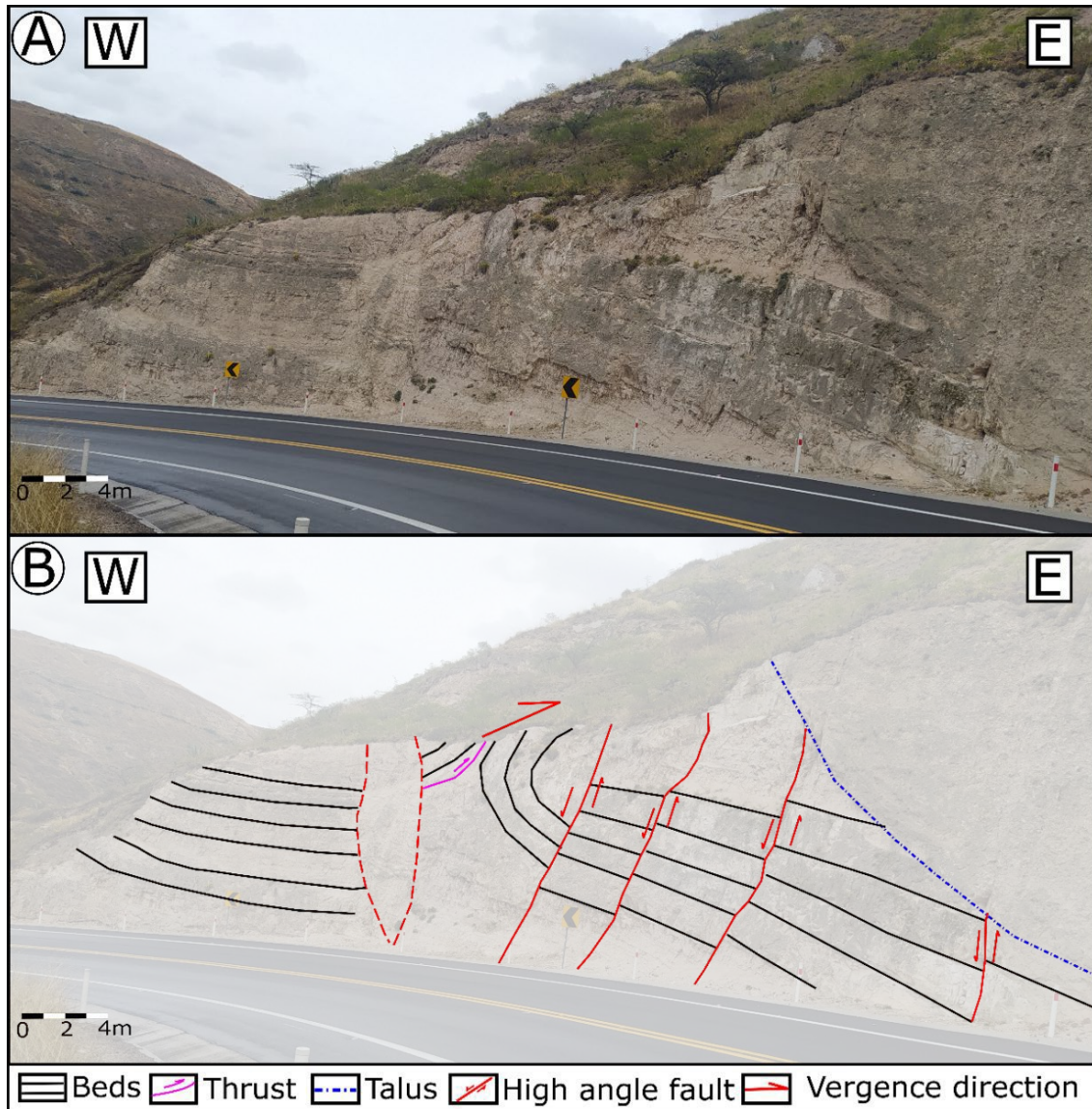


Figure 14.- (A) Outcrop W-E of the section GB5 where we observed the four white greyish overturned mudstone layers. (B) Interpretation of the outcrop GB5.

We observed that the GYBA marker is shown in the base of the outcrop GB6 towards the NW (Figure 9). Hence, the beds towards the SE are interpreted as above GYBA. We also add a detailed picture of the thrust fault ramps from GB6 (Figure 16). We also observed the hanging wall syncline, the thrust, the San Miguel-Post San Miguel unconformity, and a buttress unconformity (Figure 13). Finally, the buttress unconformity is interpreted as a syn-sedimentary normal fault because we observed the fault plane (Figure 13).

Then, we can observe more shortening structures in the outcrop GB7 (Figure 17). This figure exhibits the outcrop GB7 from a 3D model obtained after the dronefly (Figure 17A). In Figure 17B, we observed two thrusts. Then we observed a reverse fault that cut the four white greyish mudstone layers in Figure 17C. Finally, we observed the four mudstone layers folded due to a thrust Figure 17D. Finally, we observe high-angle faults that cut through the beds.

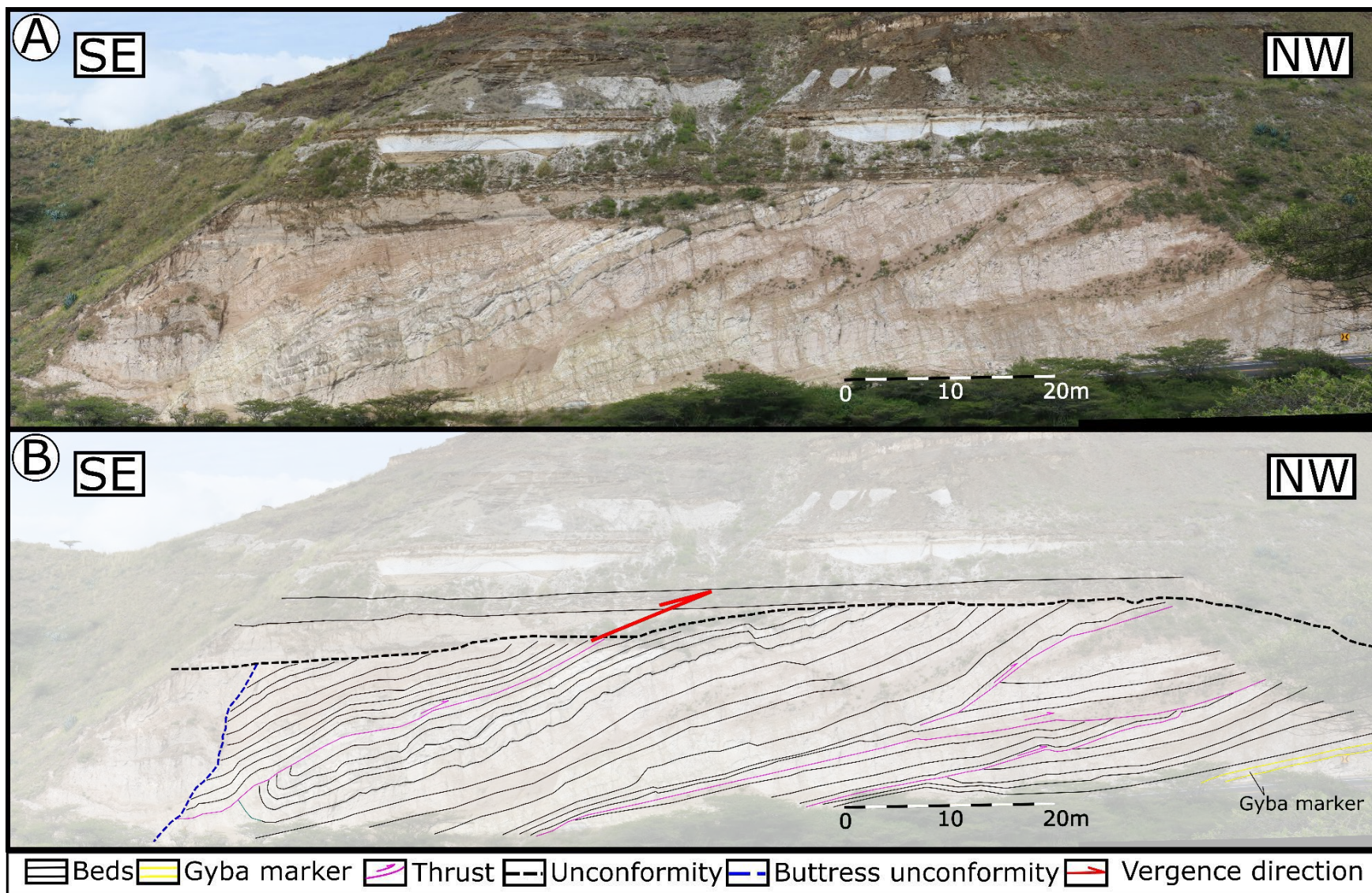


Figure 15.- (A) Outcrop SE-NW of the section GB6 exhibiting the four fault ramps sole in the decollement level at the centimetric greenish dark ash layer, the San Miguel-Post San Miguel unconformity, and the Buttress unconformity. (B) Interpretation of the outcrop GB6.

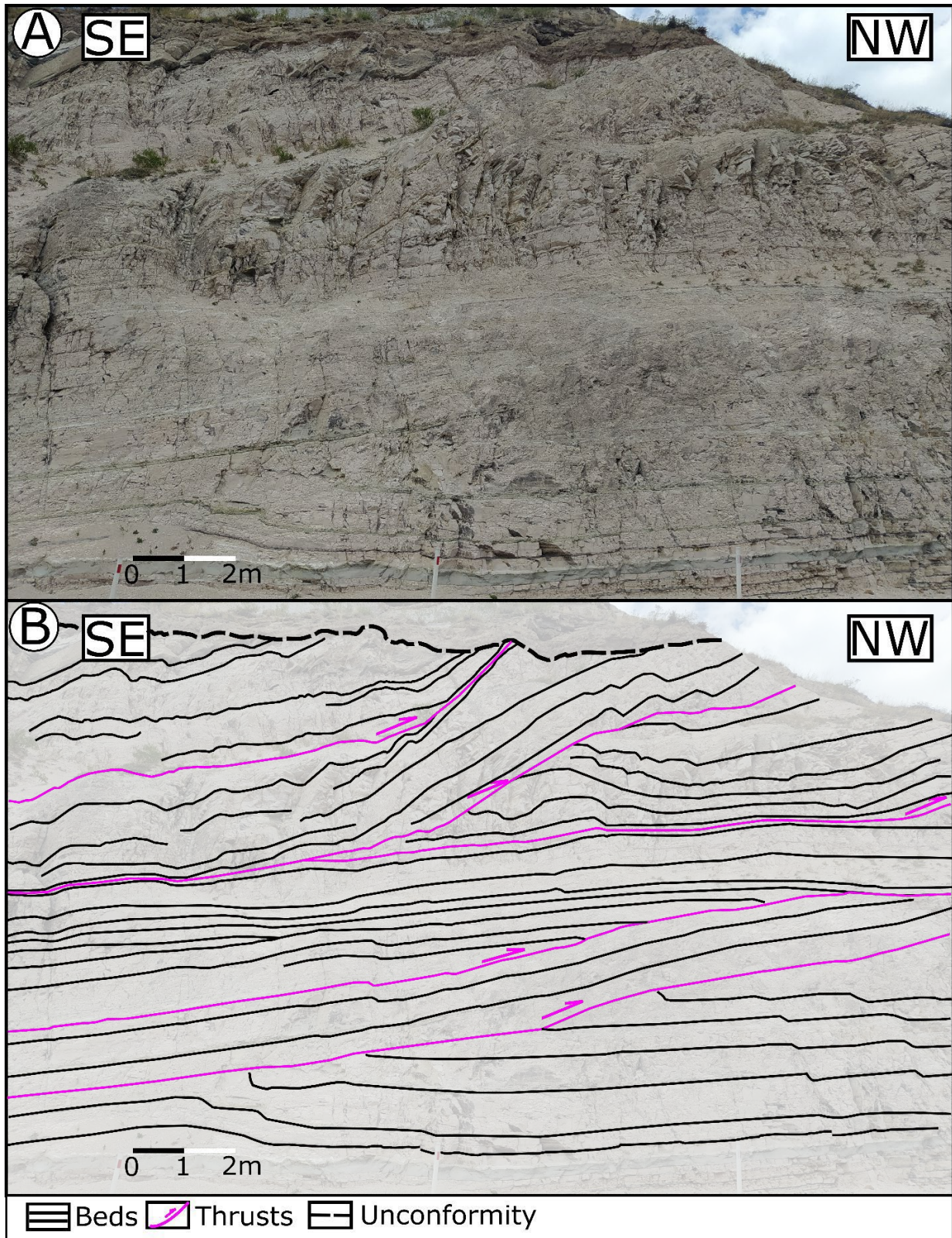


Figure 16.- (A) Outcrop SE-NW of the section GB6 where we observe fault ramps and onlap geometries within the fault ramps. (B) Interpretation of this part of the outcrop from section GB6.

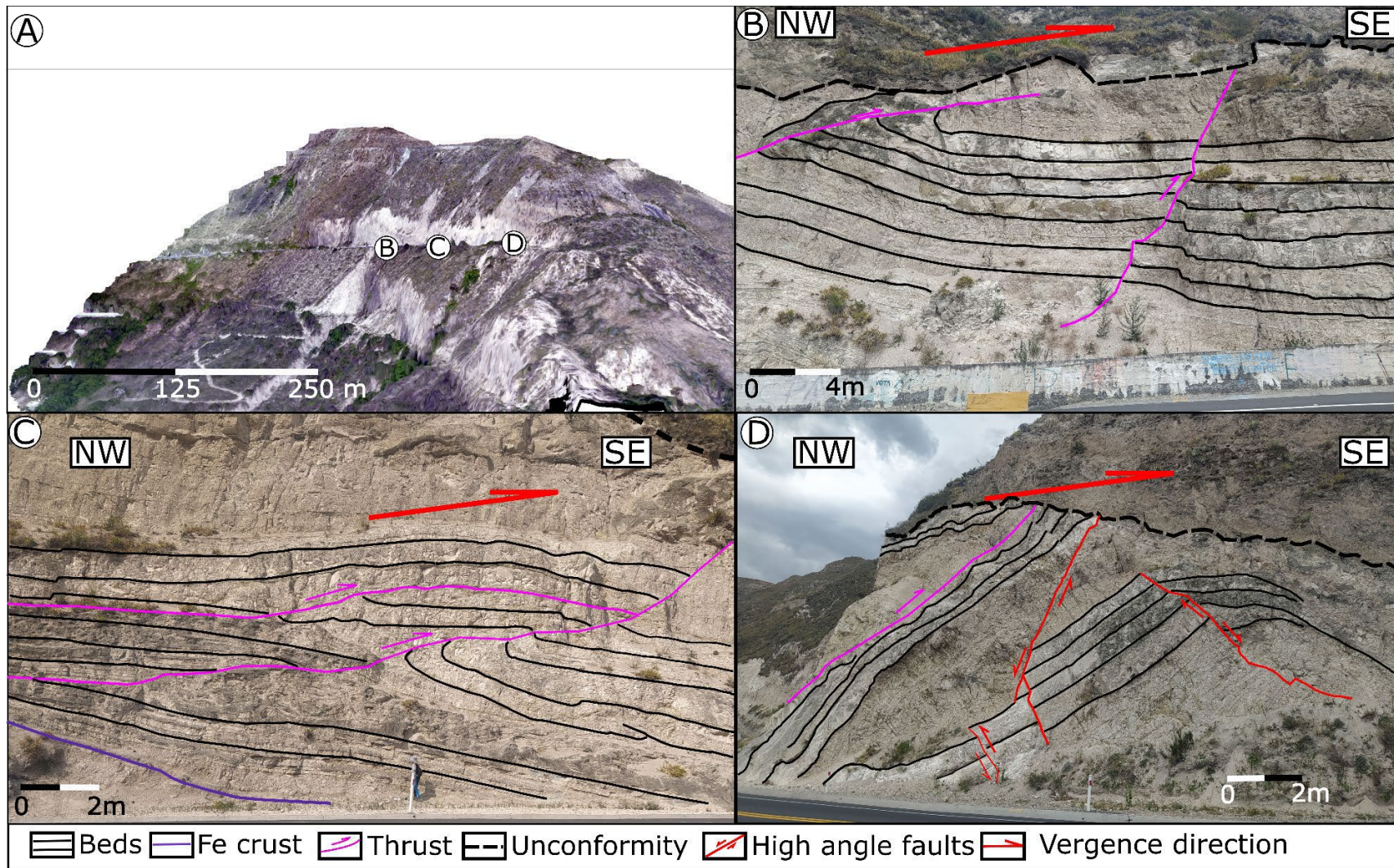


Figure 17.- (A) 3D model from the dronefly of the outcrop GB7. (B) One reverse fault that affects the four mudstone layers marker in the outcrop GB7. (C) Two thrusts found in the outcrop GB7. (D) The thrust that affected the four mudstone layers marker in the outcrop GB7.

4.3. Intensity of the deformation

The outcrops studied (Figure 7) were classified into undeformed beds, low intensity, and high intensity according to their deformation intensity. Based on the distribution of outcrops of each type, the study area was divided into regions with different intensity levels (Figure 18).

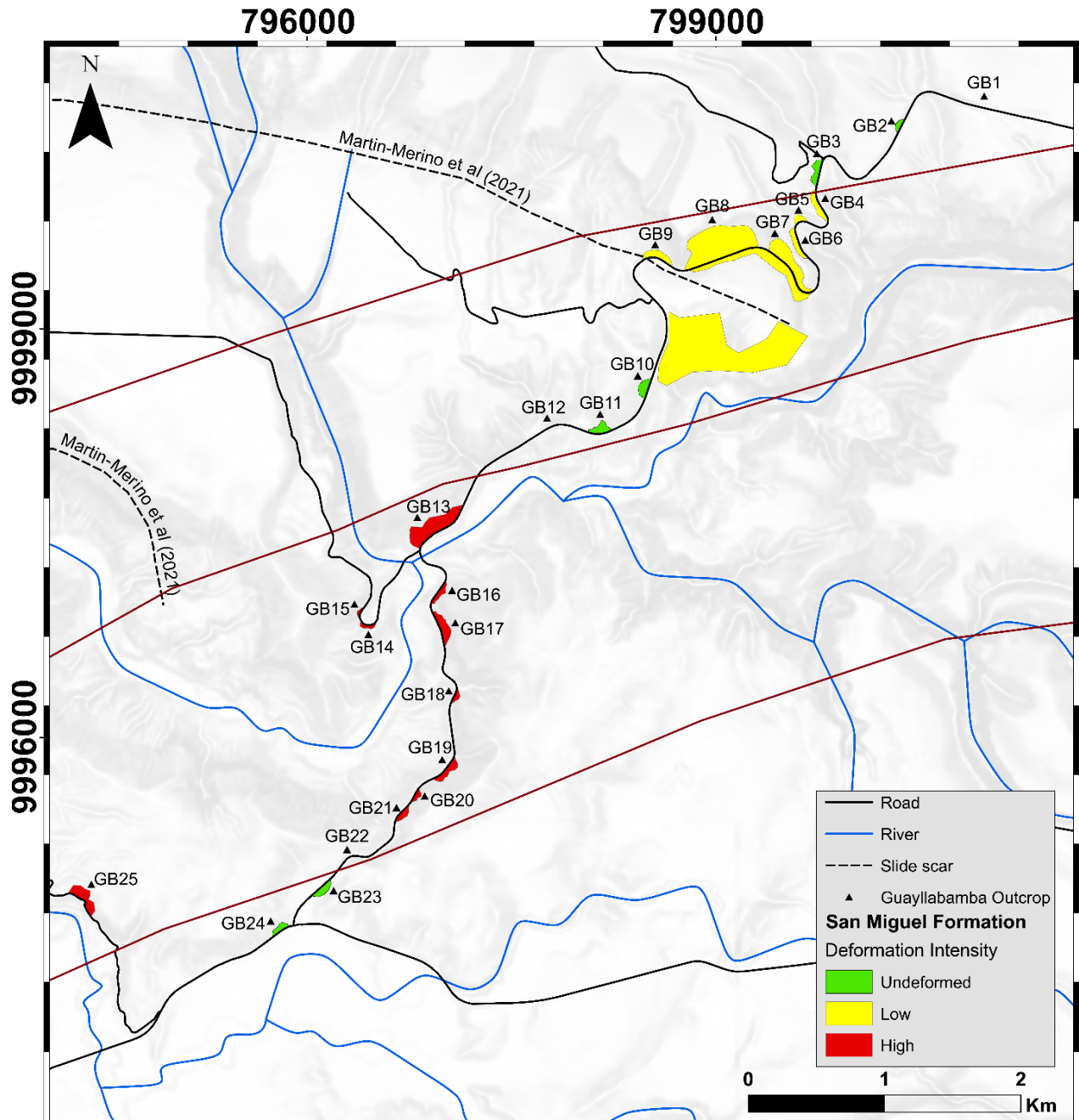


Figure 18. Map of the deformation intensity in the San Miguel Formation through the study zone where the colors describe a deformation intensity in the following way. Green: undeformed, yellow: low, and red: high. The outcrops were enclosed in areas according to their deformation intensity.

In areas where the outcrop was not accessible, the intensity of the deformation was determined with the help of binoculars. The intensity of the deformation generally increases from north to south from low to medium to high until returning to low in the southernmost region.

4.3.1. Undeformed beds

The main characteristics of the undeformed beds are low dip bed angles. The undeformed beds are located in the northeast and southeast of the study zone (Fig. 18). An example of outcrops with undeformed beds is shown in Figure 19.

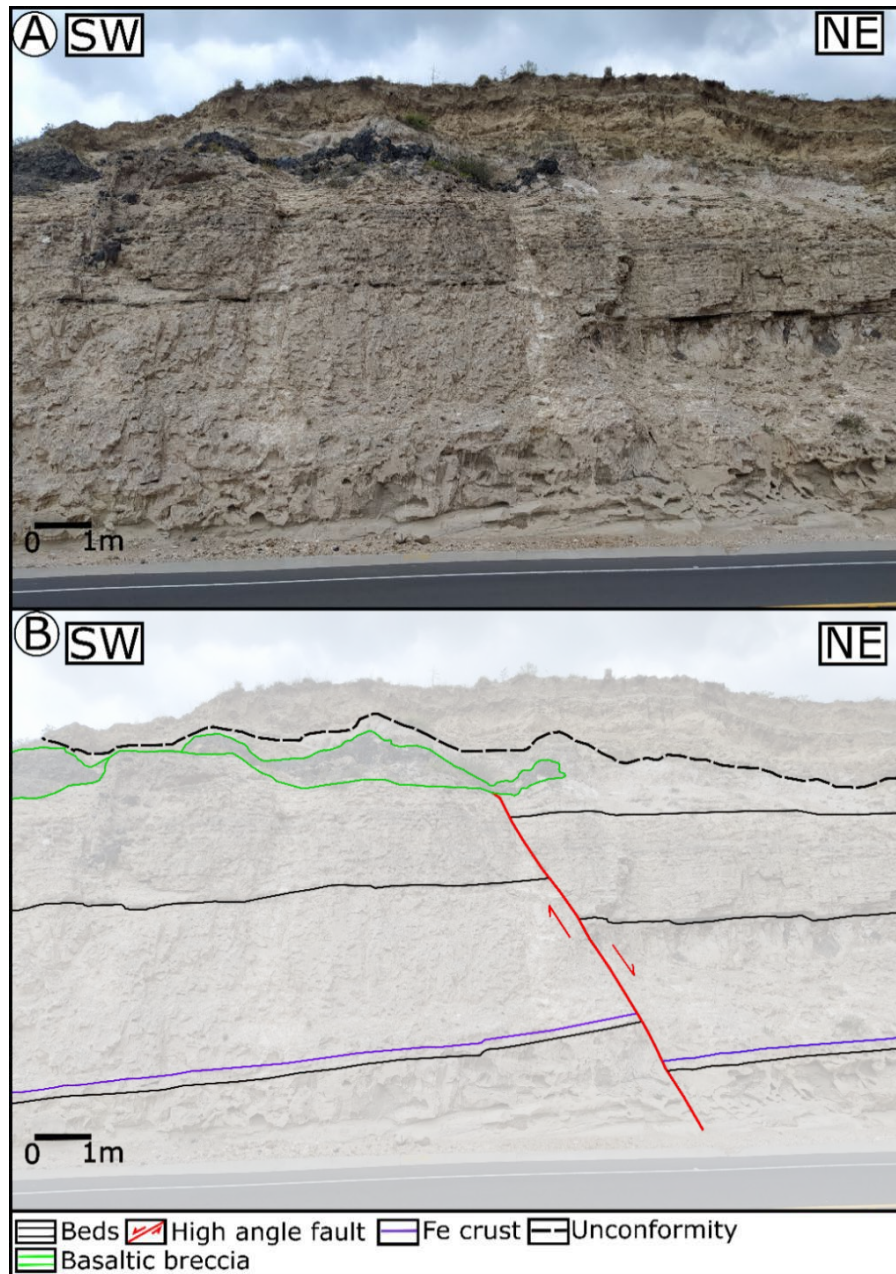


Figure 19.- (A) Outcrop SW-NE of the section GB3 where we observe undeformed beds. (B) Interpretation of the section GB3.

In Figure 19, we observed low dipping beds, the iron crust, and a basaltic breccia layer that is just seen in the northeastern part of the study zone.

4.3.2. Low-intensity deformation

This deformation intensity is characterized by beds where we observed shortening structures such as thrust with associated footwall syncline and hanging wall anticlines. We have already shown this type of deformation in Figures 9, 12, 13, 14, 15, 16, and 17. Finally, the region's location with this type of deformation can be seen in Figure 18.

4.3.3. High-intensity deformation

High-intensity deformation is characterized by medium to steeply dipping beds, synforms, antiforms, faults, folds, and thrusts, all arranged in a complex deformation pattern. Refolded folds are observed. This region with high-intensity deformation is shown in Figure 18. Examples of this deformation intensity have already been shown in Figures 10 and 11. In addition, two more outcrop examples are shown (Figures 20 and 21).

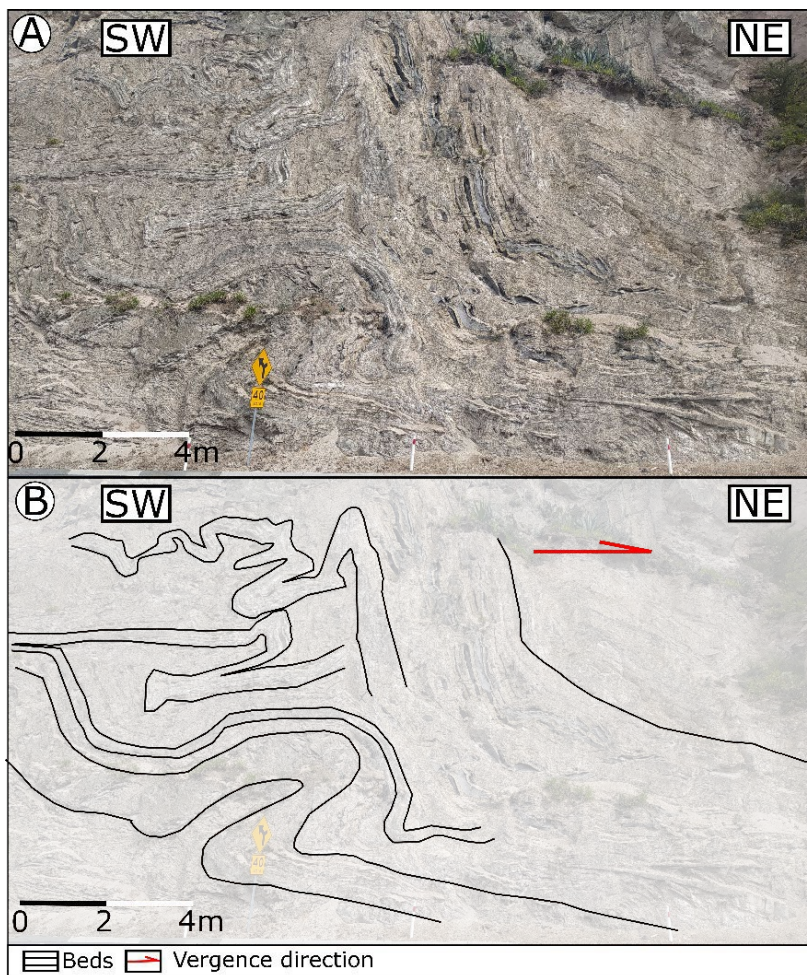


Figure 20.- (A) Outcrop SW-NE of the section Refolded GB13 where we can observe complex deformation patterns and refolded beds. (B) Interpretation of this outcrop of the section GB13.

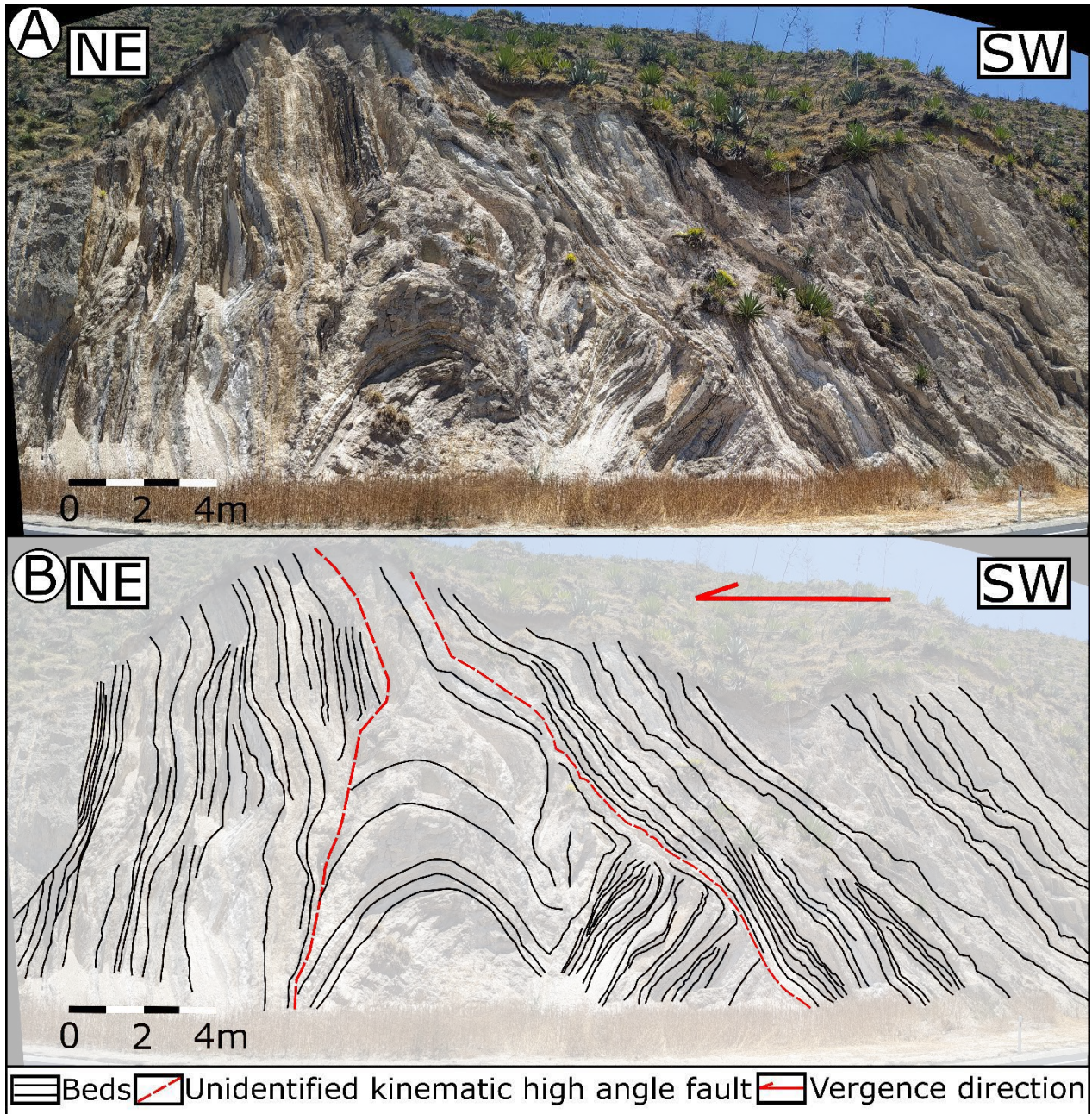


Figure 21.- (A) Outcrop NE-SW of the section GB20 where we observed antiforms, faults with unidentified kinematics, and inferred vergence direction. (B) Interpretation of the section GB20.

4.4. Vergences direction of the shortening structures

The vergence of the shortening structures was analyzed by understanding the geometries of recumbent folds, antiforms, and synforms. The vergence direction is the direction of motion of the hanging wall in trust-related folds and of the hinge in recumbent, isoclinal folds. Plane strain was assumed, and therefore the direction was interpreted as perpendicular to the fold hinges. The compiled vergence directions are shown in Figure 22.

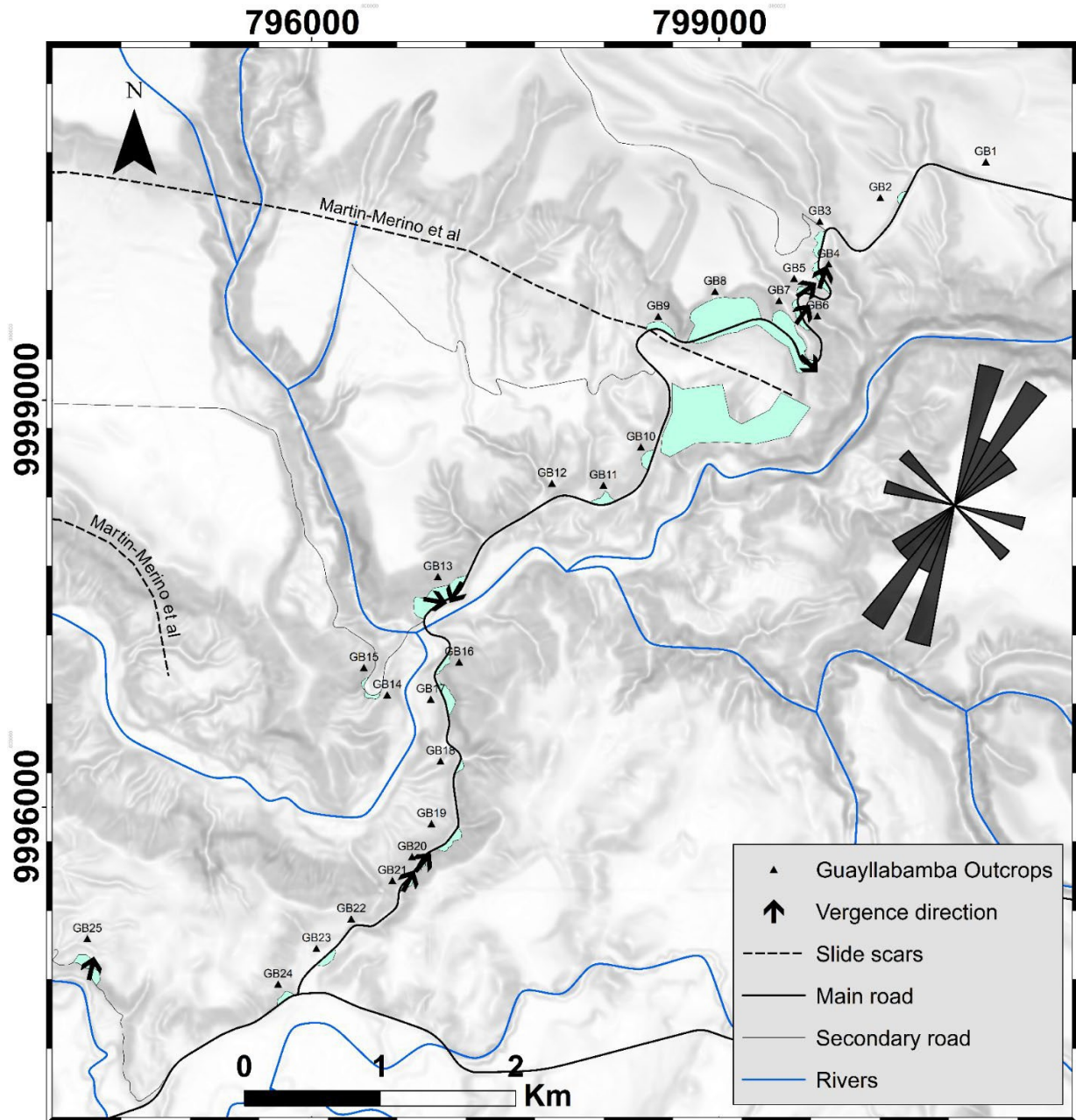


Figure 22.- Map of the shortening structures' vergence direction obtained from the field observation with a rose diagram for the vergence direction.

We observed three different vergence trends in the study zone. The first vergence direction obtained goes toward the northeast (Figures 9, 11, 14, 15, 21, and 24). The second vergence direction is southeast (Figures 17 and 20). The third vergence direction towards the southwest is already shown in Figure 23.

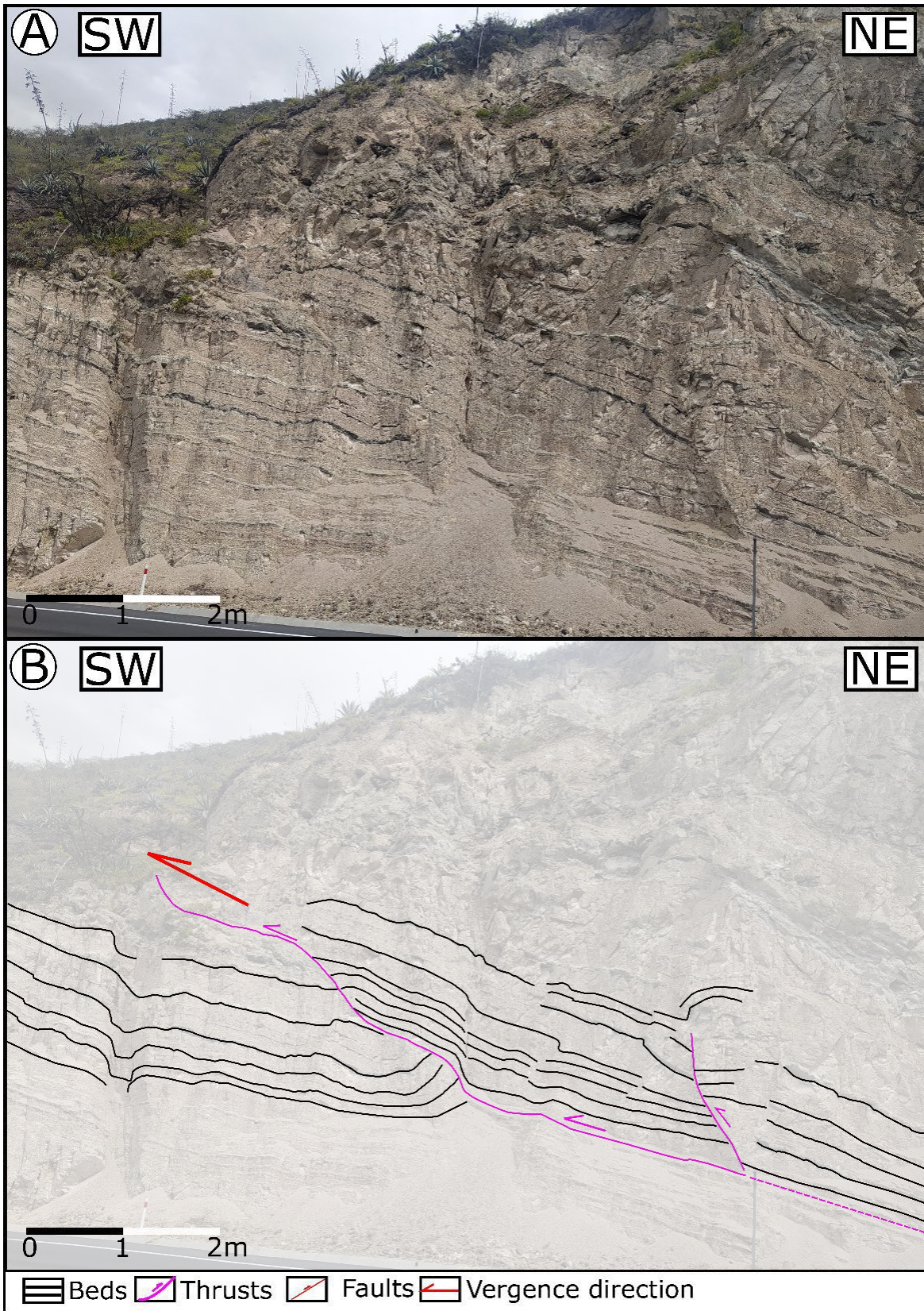


Figure 23.- (A) Outcrop SW-NE of the section GB13 above the GYBA marker with the shortening structures (footwall syncline and thrust fault) vergence direction towards the SW. (B) Interpretation of this part of the section GB13.

The vergence direction for the Figures 9, 17, and 20 was interpreted only from the transport direction of the hanging wall in thrust faults due to the lack of well-defined folds. While the vergence direction for Figures 11, 14, 15, 23, and 24 was interpreted from the direction perpendicular to the fold hinges and the hanging wall transport direction.

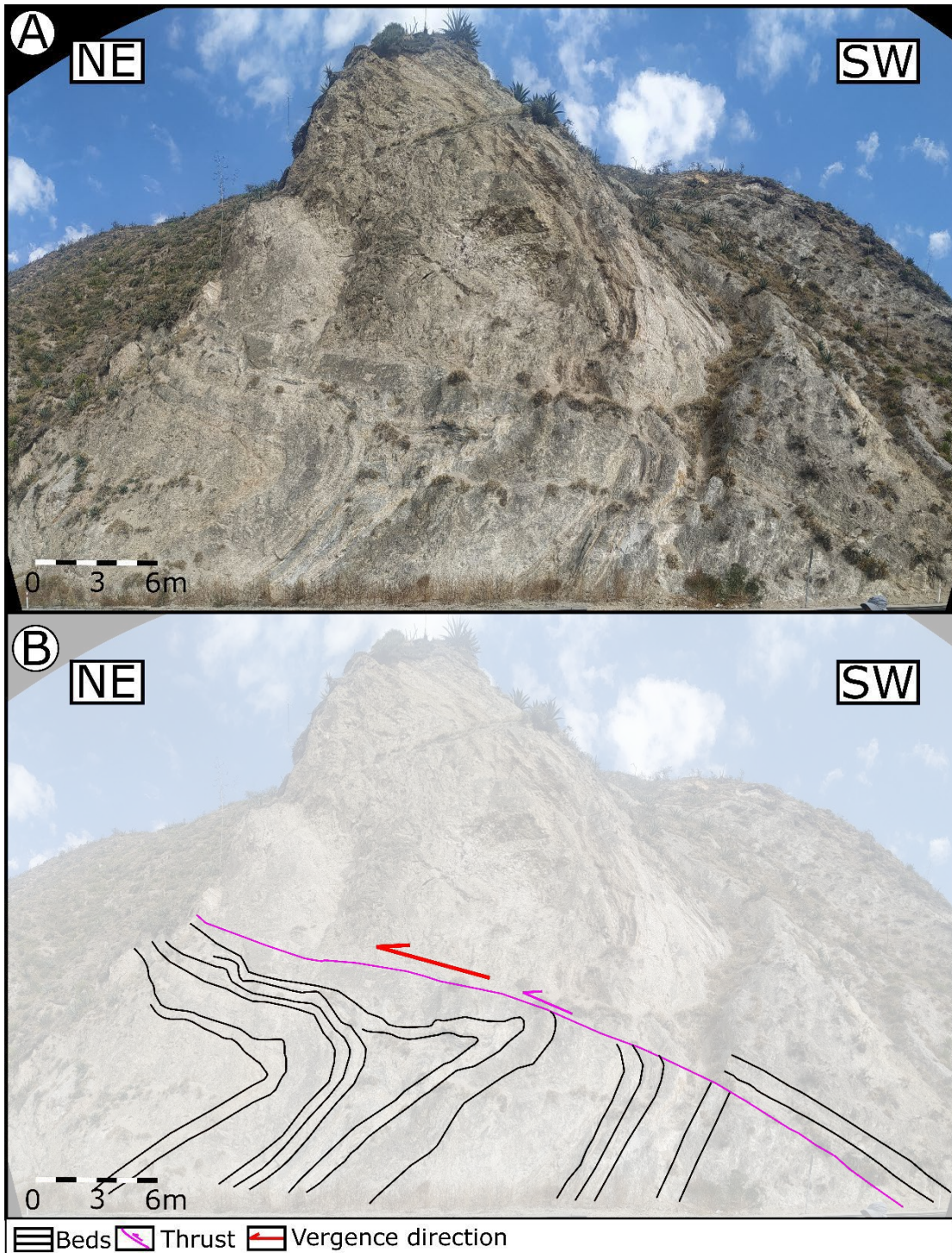


Figure 24.- (A) Outcrop GB21 (B)Outcrop GB21 where we observed an overturned fold and its vergence direction towards SW.

The vergence directions for the outcrops are summarized in Table 1:

Outcrop	Figure	Vergence direction	Position of the bodies with respect to the GYBA marker
GB4	Figure 9	18 NE	ABOVE
GB5	Figure 14	55 NE	ABOVE
GB6	Figure 15	35 NE	ABOVE
GB7	Figure 17	135 SE	ABOVE
GB13	Figure 23	210 SW	ABOVE
GB13	Figure 20	100 SE	BELOW
GB20	Figure 21	40 NE	UNIDENTIFIED
GB21	Figure 24	28 NE	UNIDENTIFIED
GB25	Figure 11	12 NE	BELOW

Table 1.- Summary of the shortening structures vergence direction with their respective figure and position to the GYBA marker.

4.5. High angle faults and surface expression related faults

We observed high angle faults younger than the shortening structures due to the cross-cutting relationship. These high-angle faults cut San Miguel formation units and are truncated by an unconformity. However, we also observed locally restricted faults that cut through Post San Miguel units and two slide scars correlated to rotational slides in the Guayllabamba basin.

4.5.1. High angle faults truncated by the unconformity

These faults get truncated by the unconformity. We mainly observed faults that have a normal throw. Some of them probably have a strike-slip component. However, we did not observe slickenlines in the field. Hence, there is no certainty about its strike-slip kinematics. We can observe examples of these faults in Figures 9, 10, 14, 17d, and 19.

4.5.2. Syn-San Miguel formation fault (Buttress unconformity)

We observed a syn-sedimentary fault that may also have represented as a buttress unconformity seen in Figures 13 and 15. This fault is also seen on the other side of the road on GB7. Hence, we show the 3D model view (Figure 25), where it is easier to interpret this fault plane on both faces of the hill.

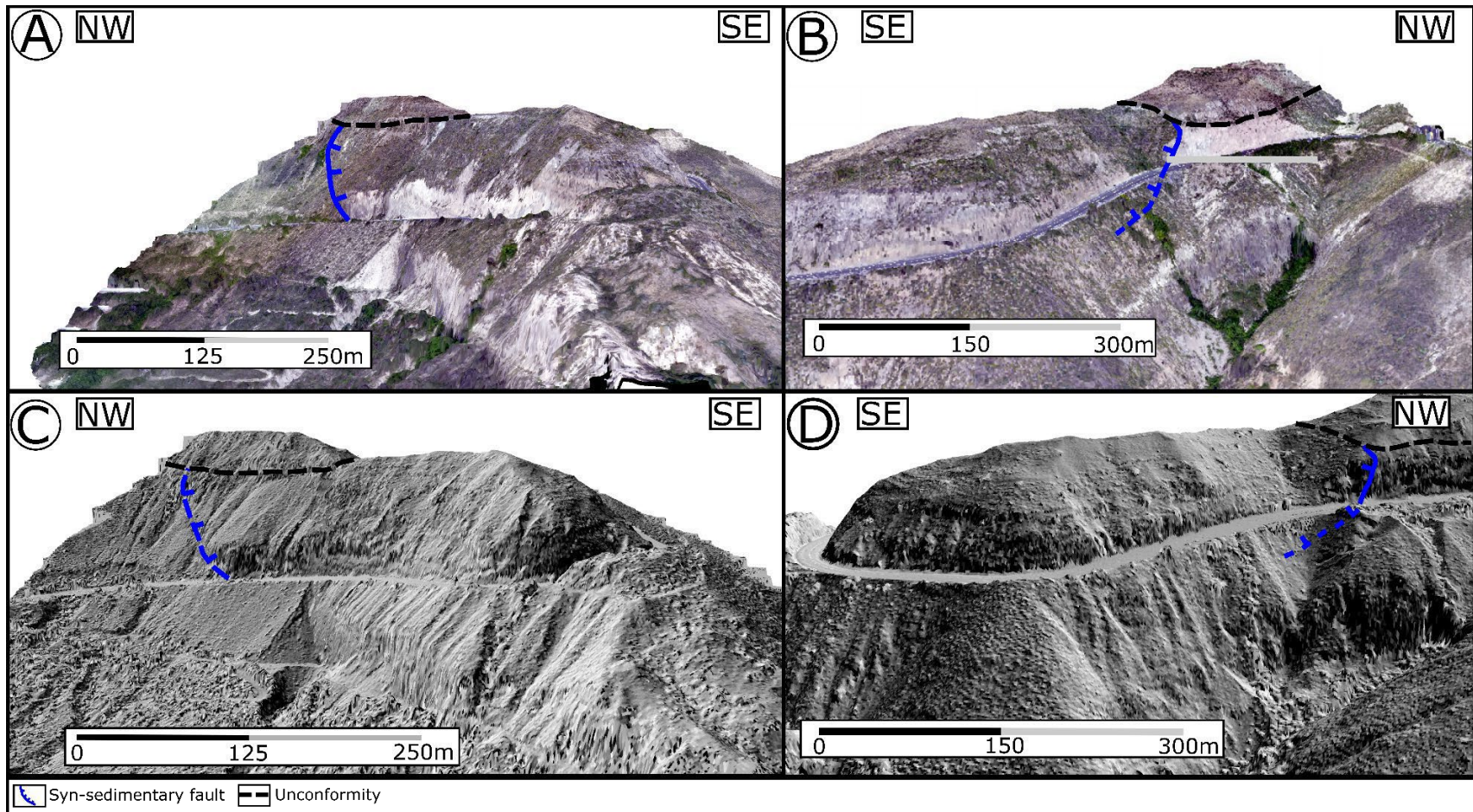


Figure 25.- (A) NW-SE Outcrop GB7 view from the 3D model with the San Miguel-post San Miguel formation unconformity and the syn-sedimentary fault. (B) SE-NW Outcrop GB6 view from the 3D model with the San Miguel-post San Miguel formation unconformity and the syn-sedimentary fault. (C) NW-SE Outcrop GB7 Hillshade view from the 3D model with the San Miguel-post San Miguel formation unconformity and the syn-sedimentary fault. (D) SE-NW Outcrop GB6 Hillshade view from the 3D model with the San Miguel-post San Miguel formation unconformity and the syn-sedimentary fault.

4.5.3. High-angle faults that cut Post San Miguel formation units.

In the northeastern part of the study zone in the outcrops GB1 and GB2, we observed Post San Miguel units and never found high angle faults cutting through them. However, we observed post-San Miguel units cut by high angle faults in the outcrop GB12 (Figure 26) and the outcrop GB23 (Figure 27).

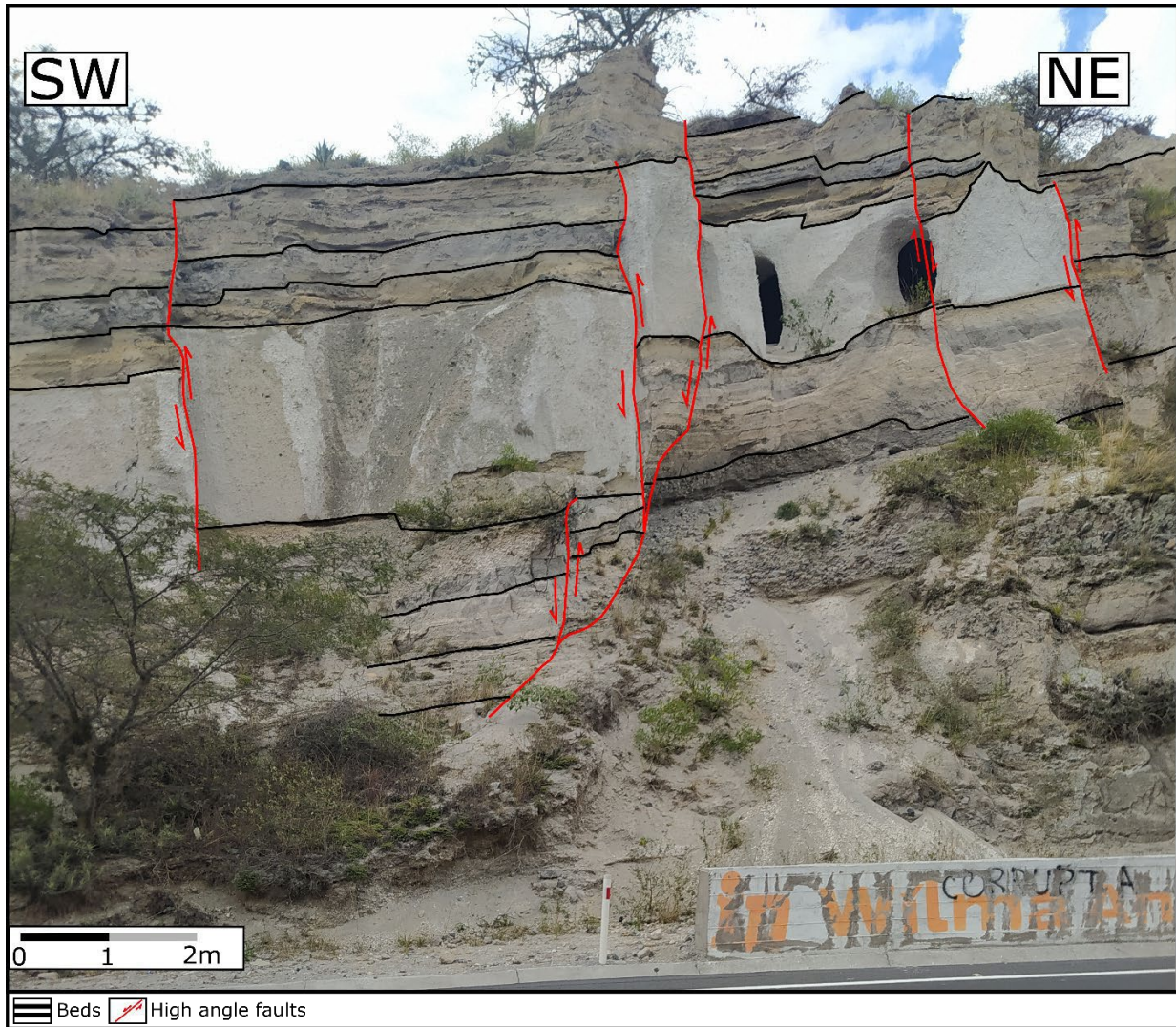


Figure 26.- High angle faults in post-San Miguel beds in the outcrop GB12

4.5.4. Slide scars related to the current Guayllabamba depression.

Finally, the two slide scars are shown in Figures 7, 18, and 22, described by (Martin et al., 2021). They can easily see from DEM view. These surface expressions can be correlated with the current Malchinguí depression and current Guayllabamba basin morphology expressions.

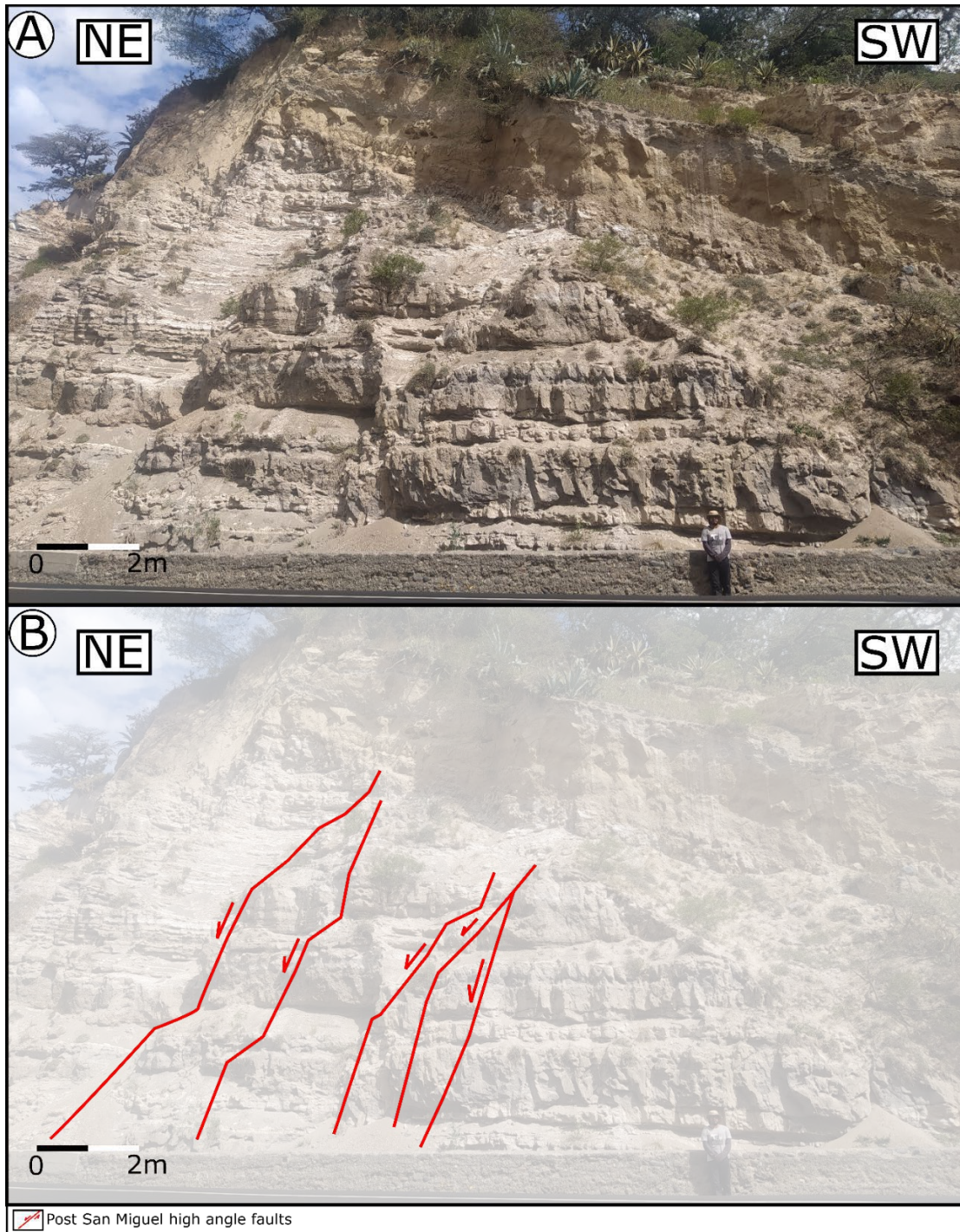


Figure 27.- High angle faults in post-San Miguel beds in the outcrop GB22.

4.6. Stereonet analysis

This section shows the stereonet results for bedding planes, fold axes, shortening structure faults, high angle faults truncated by the unconformity, high angle faults that cut through post-San Miguel units, and fractures.

4.6.1. Bedding and fold axes

One hundred twenty-seven beds were measured in the field (Figures 28A and 28B). The hinge for the fold that creates the bedding planes can be approximated by the pole of the cylindrical best fit for the poles approximating a hinge line $1 \rightarrow 319$.

Furthermore, 23-fold axes were measured in the field. The poles to the fold axial planes follow a girdle distribution when plotted on stereonet (Figures 28C).

4.6.2. Faults

4.6.2.1. Shortening structure faults

Sixteen inverse faults were recorded in the field. They are thrust and reverse faults concentrated in three clusters when plotted on stereonet (Figures 28D). The first fault cluster is represented by a plane with 334,52 NE. The second cluster is represented by a plane with 087,70 SE. Finally, the third is represented by a plane with 150,38 SW.

4.6.2.2. High angle faults truncated by the unconformity

Forty-six high-angle faults truncated by the unconformity were collected on the field. They are concentrated in three clusters when plotted in stereonet (Figure 29E). The first fault cluster can be represented by a plane dipping northwestward with 244, 73. The second cluster can be represented by a plane dipping northwestward with 197,77. Finally, the third cluster can be represented by the plane 329,65 NE. Due to the 60° angle between planes 1 and 2, we assume them to conjugate sets. The stress directions obtained are σ_1 (05 \rightarrow 222), σ_2 (72 \rightarrow 328), and σ_3 (17 \rightarrow 130).

4.6.2.1. High angle faults post-San Miguel units

Nine high-angle faults post-San Miguel units were collected on the field. They can be observed in Figure 29F. They are concentrated in one cluster that can be represented by a plane dipping northeastward with 305,71.

4.6.3. Fractures

The fracture distribution for the whole study zone is shown in Figure 29G, where 246 fractures were measured. Their orientation is concentrated in two orthogonal clusters that can be represented by a dominant plane with an orientation of 317,81 NE and a secondary plane with an orientation of 045,85 SE. Due to the 90° angle, we assume a mode one joints with σ_1 parallel to the plane 317,81 NE, σ_3 parallel to the plane 045,85 SE, and σ_2 at the intersection of both planes (80 \rightarrow 070). Due to the vertical orientation of σ_2 , we inferred a strike-slip stress state.

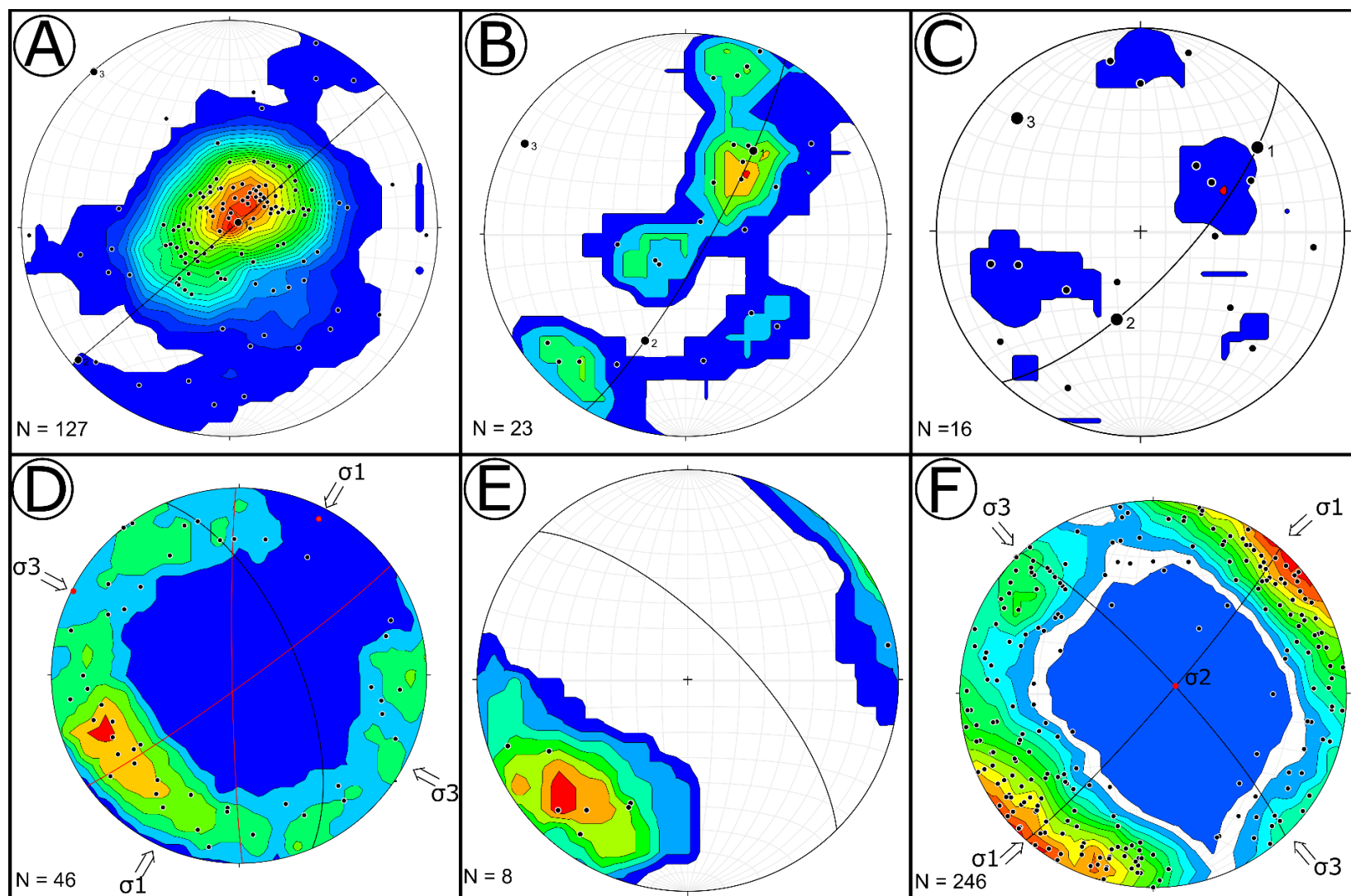


Figure 28.- Lower hemisphere, equal area projections showing (A) Kamb contouring from the bed poles of the study zone, contours are 2 sigma. (B) Kamb contouring from the poles to the fold axial planes, contours are 1 sigma. (C) Kamb contouring from thrust and reverse faults poles, contours are 2 sigmas. (D) One percent contouring from high angle fault poles truncated by the unconformity, contours are 1 sigma. The numbers 1,2 and 3 are the planes that represent the three fault clusters. (E) Kamb contouring from high angle fault poles cut through the unconformity, contours are 1 sigma. (F) Kamb contouring from fractures poles of the study zone, contours are 1 sigma.

5. Discussion

In this chapter, the structures (water escape structures, shortening structures, and high angle faults) found in the outcrops of the San Miguel Formation within the Guayllabamba basin are correlated to the different deformation events that have affected the basin. Then, we correlated the vergence direction of the shortening structures and the stereonet analysis to the olistostrome transport events. Finally, we developed a structural model for the evolution of the Guayllabamba basin.

5.1. Structures correlation to the deformation events

The water escape structure, shortening structures, syn-sedimentary San Miguel formation fault (Buttress unconformity), and high angle faults are the structures found in the San Miguel Formation within the Guayllabamba basin study zone. The water escape structure constitutes a system of clastic dykes and sills characteristic of SSD (Suter et al., 2011). They commonly develop due to fluidization in the upper parts of liquefied layers or contain impermeable laminae that create high pore pressure (Owen & Moretti, 2011). They can be triggered by an earthquake, slumping, or lateral spreading (Suter et al., 2011). Because of the stratigraphic level where this structure was found (just below the 20 meters ignimbrite layer from unit B), we can interpret this structure as triggered by the emplacement of this unit.

In general, shortening structures are related both tectonic and gravitational deformation settings. However, the structures observed in our study were considered SSD because the deformation is restricted to specific decollement levels. The decollement levels were stated above the Fe crust- below GYBA marker, above the GYBA marker, and above Fe crust- above the GYBA marker (Figure 29). In addition, the base of the deformation deepens stratigraphically towards the southwestern part of the study zone (Figure 29). Finally, the analysis of these decollement levels helped us understand the olistostrome transport direction, deformation intensity, deformation processes, and paleostresses that affected the Guayllabamba basin.

The main shortening structures observed are the thrust fault ramps that sole on a decollement level in Figures 9 and 15. The fault ramps from both outcrops (GB4 and GB6) were correlated to the same decollement level: a centimetric greenish dark ash layer where the fault ramps sole (Figure 12). We interpreted the fault ramps as a backstep thrust sequence from this data. According to

Alsop et al. (2018), the transport direction is opposite to the thrust propagation direction. Hence, the paleoslope of the olistostrome is northeastward.

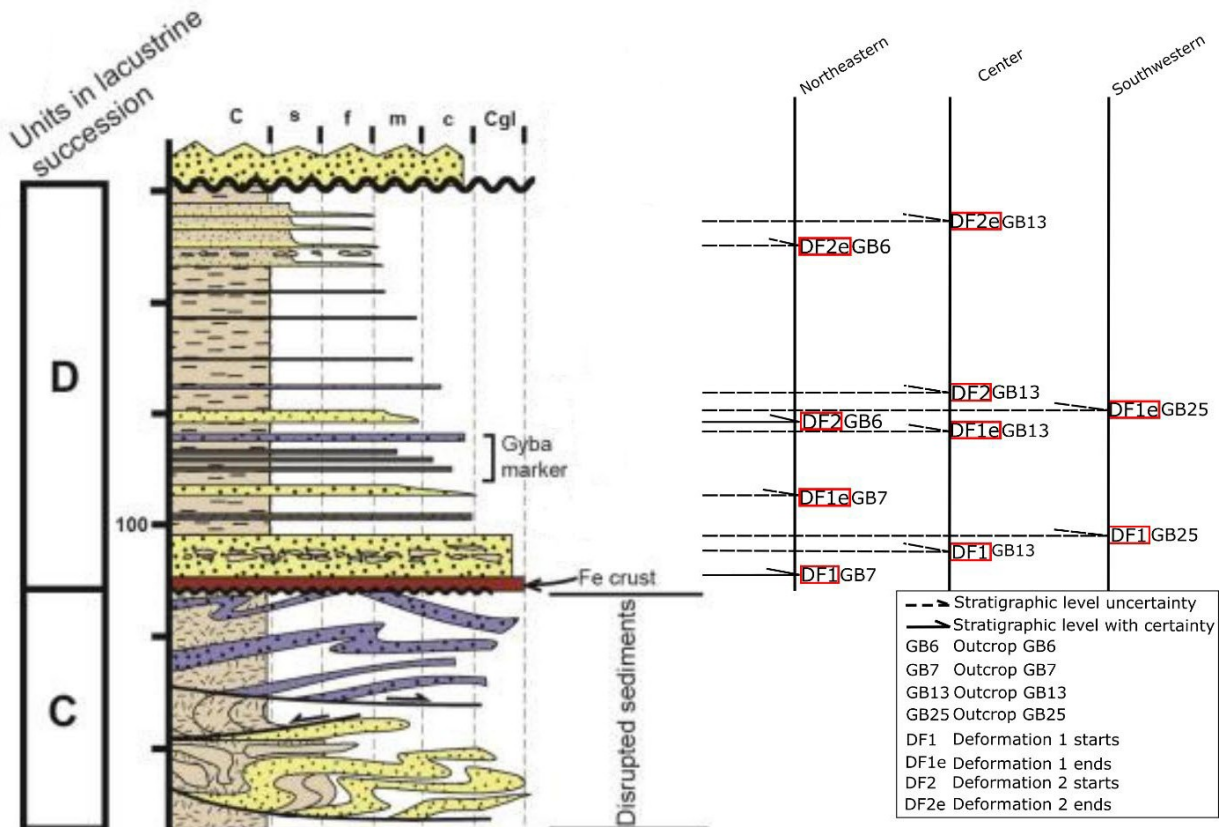


Figure 29.- Stratigraphic column of San Miguel formation units C and D, modified from Martin-Merino et al. (2021) with the deformation stages from the vergence direction towards the northeast.

In a gravitational deformation environment, we expected the deformation to move downslope, which is not consistent with the present slope of fault ramps, where the motion is updip. This difference in the expected position is explained by later tilting related to both episodes of subsequent high angle faulting delimited by the unconformity and the current rotational slide associated with the current Guayllabamba depression seen in Figures 28E and 28F.

We observed a syn-sedimentary San Miguel formation fault expressed as a Buttress unconformity. It is seen in the outcrop GB6 (Figure 13) northeastern part of the study zone, where we also observed its fault plane. It was followed below the road Figure 19 where It cuts Pisque formation but not the Golden Tuffs. According to Suter et al. (2011), a syn-sedimentary fault in the SSD context can be triggered due to an earthquake, slumps, or lateral spreading. It contains clasts of San Miguel formation in a muddy matrix truncated by the unconformity (Figure 13).

Finally, two types of high-angle faults were observed in the study zone. The high angle faults are truncated by the unconformity and the high angle faults that cut Post San-Miguel units. The high angle faults truncated by the unconformity (Figure 22E) are slightly tilted towards the northwest. The post-San Miguel faults (Figure 22F) are interpreted as less tilted than the high angle faults truncated by the unconformity. On the other hand, the two planes representing the fractures (Figure 22G) create a 90° between them, indicating a mode I joint. The stress σ_2 being almost vertical is correlated to a strike-slip stress state. Hence, we can interpret this basin as part of a transtensional tectonic setting because of the normal faulting and strike-slip stress state.

The high angle faults and the fractures along the study zone can be correlated to the collapse events of the Guayllabamba basin. However, this cannot provide us the information about the sedimentary infill from post-San Miguel units. In order to understand the dimension of the collapse, we can use the unconformity. We obtain a 350 m difference in topographic height (Figure 30) by using the unconformity height from GB8 (2397 m) and GB13 (2047 m). This topographic difference is related to the first collapse of the Guayllabamba basin. Then, we can correlate the 255m of topographic difference to the current Guayllabamba depression using the elevation profile from the line AB in Figure 30. Hence, a minimum of 105 m of post-San Miguel units had to be infilled in the Guayllabamba basin after the first collapse of the Guayllabamba depression.

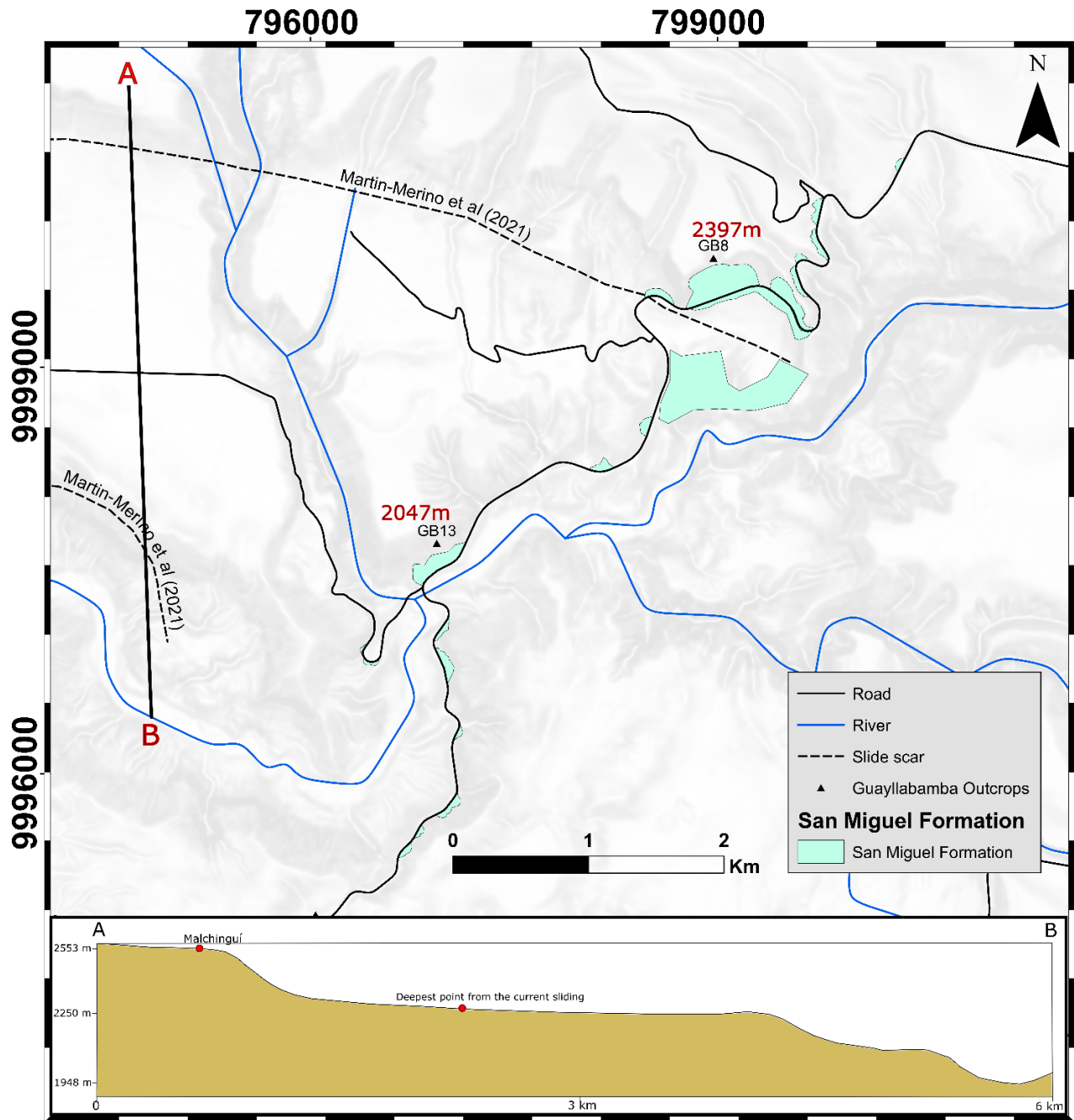


Figure 30.- Map of the study zone with an elevation profile where we observe the current Guayllabamba depression fault and the unconformity topographic difference between the outcrops GB8 and GB13. The elevation profile was made through line AB.

5.2. Shortening structures vergence correlation with the deformation events

The undeformed San Miguel formation units are concentrated in the northeastern and southeastern parts of the study zone. Then, we observe an area that concentrates the low deformed beds delimited by two red lines in the center of the basin (Figure 12). Finally, we observe the area that

concentrates the higher deformation towards the southwestern of the study zone. Hence, the intensity of deformation increases from the northeast to the southwest of the study zone. The intensity of the deformation can be correlated to the depocenter of the basin, which is consistent with the deepening trend towards the southwest of the Guayllabamba paleolake (Martin-Merino et al., 2021). Even though the stratigraphy shows that the basins deepen towards the southwest, and we expected soft-sediment deformation in that direction, this is not what we observe. Therefore, we interpret that the SSD was caused due to large-scale tilting caused by either a pull apart basin development that is consistent with our observations from fractures (strike-slip stress state) and mesoscale faults (normal faulting), or they could have been tilting related to the Quito fault. If it is the case of the Quito fault, it could be correlated with the foreland of the fault propagation fold.

Three vergence directions were obtained. The primary trend is towards the northeast. However, the other two vergences are towards the southeast and southwest. These three vergence directions could be interpreted as three different tilting events. However, the shortening structures from GB13 (Figure 20), which are taken at face value as representing opposing vergences. They are interpreted as shortening structures related to a tectonic wedge, with the southwestward vergence direction being an apparent motion on a passive roof thrust, as shown in Figure 31.

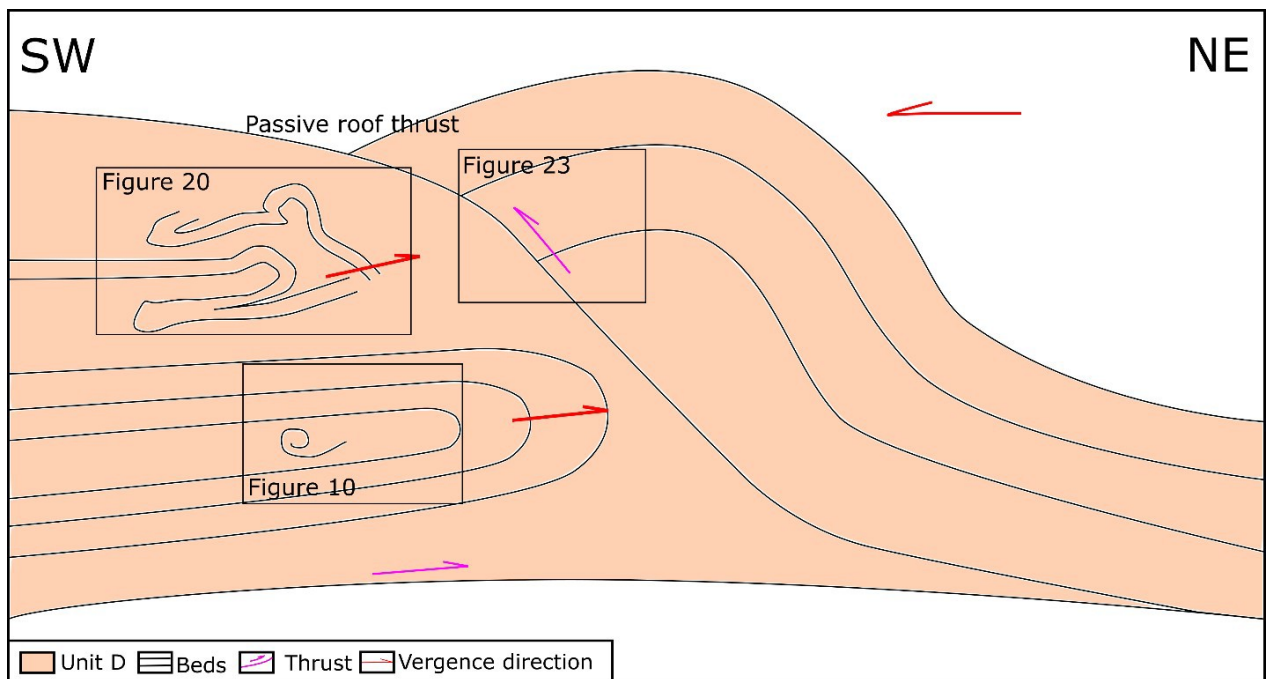


Figure 31.- Sketch of the tectonic wedge created in the middle of the basin outcrop GB13 (See location in Figure 7) where we can correlate the structures to Figures 10, 20, and 23.

Moreover, the southeastward vergence direction from the outcrops GB7 and GB13 are possible just one rotation related to the later high angle faulting. Hence, the interpretation is that this mass transport deposit had an average paleoslope towards the northeast.

5.3. Model of the structural evolution from the Guayllabamba basin

The history of the Guayllabamba basin starts from the basal lava flows dated 2.25 ± 0.5 Ma (OLADE-INECEL, 1980), 2.6 ± 0.06 , and 3.46 ± 0.1 Ma (Barberi et al., 1988). Over this, the Golden tuff was unconformably formed. Then, fluvial succession of early Pisque is deposited (Martin-Merino et al., 2021; Villagómez, 2003). Then, the Upper Pisque and San Miguel formations were concordantly deposited over Early Pisque, which is studied in detail.

1.- Unit A (Upper Pisque formation) and B were deposited. The soft-sediment deformation does not occur until the clastic dyke and sills below the Fe crust. The clastic dykes and sills were triggered due to an earthquake or the deposition of the slumped beds from unit B before the ignimbrite. The units are dipping toward the southwest (Figure 32A).

2.- The unconsolidated sediments from unit C were deposited and sedimented. Then, unit D is deposited. Then, the units get tilted towards the northeast due to the pull-apart basin development or the foreland of the Quito fault propagation fold.

3.- The units get transported towards the northeast (Figure 32B) in three different decollement levels: dec1, dec2, and dec3 (see Figure 32A). Its paleoslope indicates that the olistostrome continued in the same direction towards the northeast—the fault ramps sole on the same decollement as shown in Figures 9 and 15. While the transport direction is towards the northeast, the thrust propagation direction is towards the southwest. The thrust model is interpreted as an overstep thrust sequence (see Figure 5D). Next, the thrust propagation creates a tectonic wedge in the center of the basin, as shown in Figure 30. This tectonic wedge is responsible for the apparent olistostrome transport direction towards the southwest from the outcrop GB13 (see location in Figure 22).

4.- The syn-sedimentary San Miguel fault expressed as Buttress unconformity occurred (Figure 13).

5.- The first extension of the Guayllabamba basin occurred (Figure 32C) and is recorded in the high faults truncated by the unconformity (Figure 28E). After this collapse of the basin, an unconformity forms truncating the stratigraphy and faults underlying it.

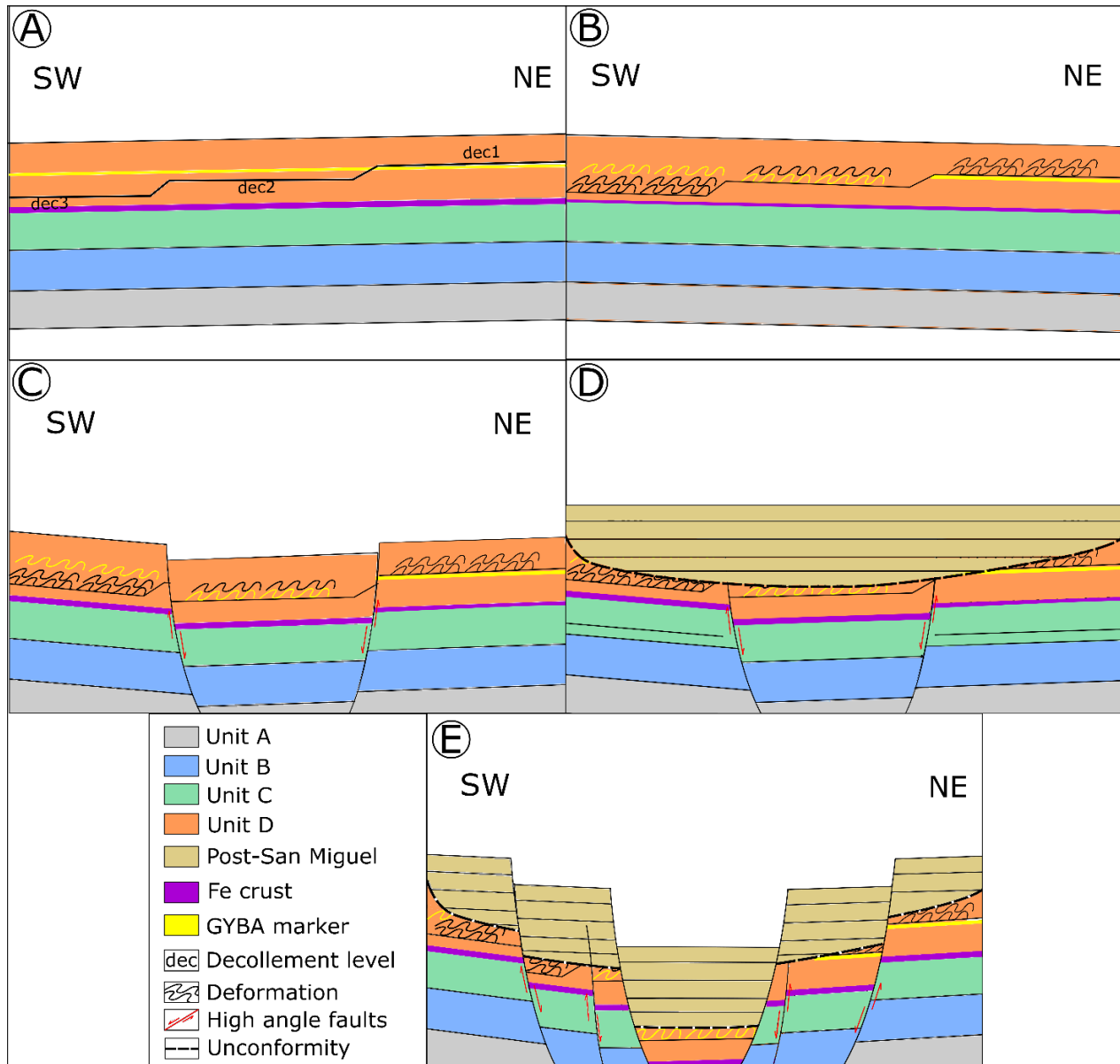


Figure 32.- Simplified model of the tectonic-structural evolution from the Guayllabamba basin. (A). The units A, B, C, and D are deposited, and the four decollement levels are stated. (B). The decollement level with its respective deformation occurred. (C). The first extension of the Guayllabamba basin occurred. (D). The upper part of the San Miguel formation is eroded and unconformably deposited by the post-San Miguel units. (E). The current Guayllabamba collapse occurred.

6. The post-San Miguel units are deposited in the resulting paleovalley and fill the existing relief as evidenced by the onlap surface developed on the unconformity (Figure 32D). The latest dated units are Late-Pleistocene units correlated to the Mojanda volcanic complex: 0.59 ± 0.06 Ma and 0.5 ± 0.06 Ma, K/Ar whole-rock andesite (Barberi et al., 1988).

7.- The second collapse of the Guayllabamba basin occurred (Figure 32E). It is recorded by the high angle faults (Figure 28F) that limit the large rotational landslide that forms the current Guayllabamba depression and that form prominent slide scarps (Martin-Merino et al., 2021).

6. Conclusion

The deformation of the Upper Pisque (unit A) and San Miguel formation (units B, C, and D) along the Tabacundo-Guayllabamba road was characterized through the recompilation of structural data and field descriptions. These units were recorded in the maps from Figures 7, 18, and 22. The deformation intensity of the outcrops increases from the northeast of the study zone to the southwest of the study zone. In contrast, the deformation intensity decreases in the southeastern of the study zone, as shown in Figure 18.

In addition, a paleoslope map was obtained from the vergence direction of the shortening structures (Figure 22). It helped understand the olistostrome transport direction towards the northeast and the apparent movement towards the southwest related to a tectonic wedge that creates passive roof thrust shown in Figure 30. Also, the geometry from the fold from outcrop GB6 and GB7 that affect the four white greyish mudstone marker was better understood through the use of the 3d model created from the drone-captured imagery and photogrammetric techniques, as is shown in Figure 25. Furthermore, the analysis of the structural data and the pictures taken in the field helped us understand the deformation processes (olistostrome transport towards the northeast) and the paleostresses that affected the formation of the Guayllabamba basin. Paleostresses such as the one that affected the first high angle faulting of the basin truncated by the unconformity and the later post-San Miguel units high angle faulting.

Finally, a model of the tectonic-structural evolution from the Guayllabamba basin was created. The basin laid over the basal lava flows dated 2.25 ± 0.5 Ma (OLADE-INECEL, 1980), 2.6 ± 0.06 , and 3.46 ± 0.1 Ma (Barberi et al., 1988). Then, the Golden Tuffs and the early Pisque formation were deposited. Next, units A and B were deposited and sediment until an earthquake or the emplacement of the disrupted sediments from unit B let the formation from the clastic dykes and sills system. Then, the unconsolidated sediments from unit C until the layers above Fe crust were deposited and sedimented. These layers are gravitationally deformed and transported toward the northeast until this event is stopped. Next, an extension event occurred, and the first high angle faulting occurred. Next, the post-San Miguel units get deposited and sedimented. The last dated units are 0.59 ± 0.06 Ma and 0.5 ± 0.06 Ma, K/Ar whole-rock andesite (Barberi et al., 1988). Finally, the second extension of the Guayllabamba basin occurred, and it is correlated to the current Guayllabamba depression is shown as slide scarps (Martin-Merino et al., 2021)

7. Recommendations

This study gets limited in understanding the ages of the San Miguel Formation and the understanding of the post-San Miguel units. It also gets limited in the complete understanding of the geometrical relation of the fold near the Pisque river viewpoint. Thus, the following recommendation is hereby presented:

- Conduct geochronologic dating from the San Miguel units because they lack age information to constrain the collapse of the Guayllabamba basin.
- Create detailed stratigraphic columns of the post-San Miguel units to understand better the sedimentary processes that act over these units.
- Fly a drone to create a two-sided 3D model of the fold near the Pisque river viewpoint

8. Bibliography

- Alsop, G. I., & Marco, S. (2013). Seismogenic slump folds formed by gravity-driven tectonics down a negligible subaqueous slope. *Tectonophysics*, 605, 48–69. <https://doi.org/10.1016/j.tecto.2013.04.004>
- Alsop, G. I., Weinberger, R., & Marco, S. (2018). Distinguishing thrust sequences in gravity-driven fold and thrust belts. *Journal of Structural Geology*, 109, 99–119. <https://doi.org/10.1016/j.jsg.2018.01.005>
- Alvarado, A., Audin, L., Nocquet, J. M., Jaillard, E., Mothes, P., Jarrín, P., Segovia, M., Rolandone, F., & Cisneros, D. (2016). *Partitioning of oblique convergence in the Northern Andes subduction zone: Migration history and the present-day boundary of the North Andean Sliver in Ecuador*. 2, 1048–1065. <https://doi.org/10.1002/2016TC004117>. Received
- Aspden, J. A., & Litherland, M. (1992). The geology and Mesozoic collisional history of the Cordillera Real, Ecuador. *Tectonophysics*, 205(1–3), 187–204. [https://doi.org/10.1016/0040-1951\(92\)90426-7](https://doi.org/10.1016/0040-1951(92)90426-7)
- Barberi, F., Coltelli, M., Ferrara, G., Innocenti, F., Navarro, J. M., & Santacrose, R. (1988). Plio-Quaternary volcanism in Ecuador. *Geological Magazine*, 125(1), 1–14. <https://doi.org/10.1017/S0016756800009328>
- Barragán, R., Baudino, R., & Marocco, R. (1996). Geodynamic evolution of the Neogene intermontane Chota basin, Northern Andes of Ecuador. *Journal of South American Earth Sciences*, 9(5–6), 309–319. [https://doi.org/10.1016/s0895-9811\(96\)00016-8](https://doi.org/10.1016/s0895-9811(96)00016-8)
- Benitez, S. (1995). *Évolution géodynamique de la province côtière sud-équatorienne au Crétacé supérieur Tertiaire*. Université Joseph-Fourier- Grenoble I.
- Camerlenghi, A., & Pini, G. A. (2009). Mud volcanoes, olistostromes and Argille scagliose in the Mediterranean region. *Sedimentology*, 56(1), 319–365. <https://doi.org/10.1111/j.1365-3091.2008.01016.x>
- DeMets, C., Gordon, R. G., Argus, D. F., & Stein, S. (1990). Current plate motions. *Geophysical Journal International*, 101(2), 425–478. <https://doi.org/10.1111/j.1365-246X.1990.tb06579.x>
- DGGM. (1977). *Hoja geológica “El Quinche”. Escala 1:50000*.
- DGGM. (1982). *Hoja geológica “El Quinche”. Escala 1:25000*.
- Ego, F., Sébrier, M., Lavenu, A., Yepes, H., & Egues, A. (1996). Quaternary state of stress in the Northern Andes and the restraining bend model for the Ecuadorian Andes. *Tectonophysics*, 259(1-3 SPEC. ISS.), 101–116. [https://doi.org/10.1016/0040-1951\(95\)00075-5](https://doi.org/10.1016/0040-1951(95)00075-5)

- Farrell S. (1984). A dislocation model applied to slump structures, Ainsa Basin, South Central Pyrenees. *Journal of Structural Geology*, 6(6), 727–736.
- Gutscher, M., Malavieille, J., Lallemand, S., & Collot, J. (1999). Tectonic segmentation of the North Andean margin : impact of the Carnegie Ridge collision. *Earth and Planetary Science Letters*, 168, 255–270.
- Hughes, R. A., & Pilatasig, L. F. (2002). Cretaceous and tertiary terrane accretion in the Cordillera Occidental of the Andes of Ecuador. *Tectonophysics*, 345(1–4), 29–48. [https://doi.org/10.1016/S0040-1951\(01\)00205-0](https://doi.org/10.1016/S0040-1951(01)00205-0)
- Kellogg, J. N., Vega, V., Stailings, T. C., & Aiken, C. L. V. (1995). Tectonic development of Panama, Costa Rica, and the Colombian Andes: Constraints from Global Positioning System geodetic studies and gravity. *Special Paper of the Geological Society of America*, 295, 75–90. <https://doi.org/10.1130/SPE295-p75>
- Lavenu, A., Baudino, R., & Ego, F. (1996). Stratigraphie des depots Tertiaires et Quaternaires de la Depression Interandine d'Equateur (entre 0° et 2°15'S). *Bulletin - Institut Francais d'Etudes Andines*, 25(1), 1–15.
- Litherland, M. (1994). The metamorphic belts of Ecuador. *British Geological Survey Overseas Memoir*, 11.
- Maltman, A. (1987). *Shear zones in argillaceous sediments an experimental study*. <http://sp.lyellcollection.org/>
- Martin-Merino, G., Almeida, R., & Roverato, M. (2021). *Volcaniclastic lacustrine sedimentation in the Pleistocene Guayllabamba intermontane basin in the Ecuadorian Andes*.
- Nocquet, J., Chlieh, M., Mothes, P. A., Rolandone, F., Jarrin, P., Cisneros, D., Alvarado, A., Audin, L., Bondoux, F., Martin, X., Font, Y., Régnier, M., Vallée, M., Tran, T., Beauval, C., Mendoza, J. M. M., Martinez, W., Tavera, H., & Yepes, H. (2014). Motion of continental slivers and creeping subduction in the northern Andes. *Nature Geoscience*, 7(March). <https://doi.org/10.1038/NGEO2099>
- Norabuena, E. O., Dixon, T. H., Stein, S., & Harrison, G. A. (1999). *Decelerating Nazca-South America and Nazca-Pacific Plate motions*. 26(22), 3405–3408.
- OLADE-INECEL. (1980). *Informe geo-volcanológico: proyecto de investigación geotérmica de la República del Ecuador*.
- Owen, G., & Moretti, M. (2011). Identifying triggers for liquefaction-induced soft-sediment deformation in sands. *Sedimentary Geology*, 235(3–4), 141–147. <https://doi.org/10.1016/j.sedgeo.2010.10.003>

- Pardo-Casas, F., & Molnar, P. (1987). Relative motion of the Nazca (Farallon) and South American Plates since Late Cretaceous time. *Tectonics*, 6(3), 233–248.
- Reinoso, M. (2021). *Stratigraphic and tectonic characterization of the Peñas Coloradas Formation, and its relation with the deposits of the Chota formation in the Chota Basin of northern Ecuador Trabajo de integ.* Yachay Tech University.
- Robin, C., Hall, M., Jimenez, M., Monzier, M., & Escobar, P. (1997). Mojanda volcanic complex (Ecuador): development of two adjacent contemporaneous volcanoes with contrasting eruptive styles and magmatic suites. *Journal of South American Earth Sciences*, 10(5–6), 345–359. [https://doi.org/10.1016/S0895-9811\(97\)00030-8](https://doi.org/10.1016/S0895-9811(97)00030-8)
- Samaniego, P., Egues, A., Hibsich, C., Villagómez, R., & Segovia, M. (1994). Estratigrafía y tectónica de la Cuenca de Guayllabamba. *Terceras Jornadas En Ciencias de La Tierra*, 49–50.
- Spikings, R. A., Seward, D., Winkler, W., & Ruiz, G. M. (2000). *Low-temperature thermochronology of the northern Cordillera Real, Ecuador: Tectonic insights from zircon and apatite fission track analysis*. 19(4), 649–668.
- Spikings, R. A., Winkler, W., Hughes, R. A., & Handler, R. (2005). Thermochronology of allochthonous terranes in Ecuador: Unravelling the accretionary and post-accretionary history of the Northern Andes. *Tectonophysics*, 399(1-4 SPEC. ISS.), 195–220. <https://doi.org/10.1016/j.tecto.2004.12.023>
- Spikings, R., Paul, A., Vallejo, C., & Reyes, P. (2021). Constraints on the ages of the crystalline basement and Palaeozoic cover exposed in the Cordillera real, Ecuador: $^{40}\text{Ar}/^{39}\text{Ar}$ analyses and detrital zircon U/Pb geochronology. *Gondwana Research*, 90, 77–101. <https://doi.org/10.1016/j.gr.2020.10.009>
- Streit, R. L., Burbank, D. W., Strecker, M. R., Alonso, R. N., Cottle, J. M., & Kylander-Clark, A. R. C. (2017). Controls on intermontane basin filling, isolation and incision on the margin of the Puna Plateau, NW Argentina (~23°S). *Basin Research*, 29, 131–155. <https://doi.org/10.1111/bre.12141>
- Tibaldi, A., & Ferrari, L. (1992). From latest miocene thrusting to quaternary transpression and transtension in the Interandean Valley, Ecuador. *Journal of Geodynamics*, 15(1–2), 59–83. [https://doi.org/10.1016/0264-3707\(92\)90006-E](https://doi.org/10.1016/0264-3707(92)90006-E)
- Vallejo, C. (2007). *Evolution of the Western Cordillera in the Andes of Ecuador (Late Cretaceous-Paleogene)* [Doctoral Thesis]. Swiss Federal Institute of Technology Zurich.
- Vallejo, C., Winkler, W., Spikings, R. A., Luzieux, L., Heller, F., & Bussy, F. (2009). Mode and timing of terrane accretion in the forearc of the Andes in Ecuador. *Memoir of the Geological Society of America*, 204(09), 197–216. [https://doi.org/10.1130/2009.1204\(09\)](https://doi.org/10.1130/2009.1204(09))

- Villagómez, D. (2003). *Evolución Geológica Plio-Cuaternaria del valle interandino central en Ecuador (Zona de Quito Guayllabamba-San Antonio)* [Ungergraduate thesis]. Escuela Politécnica Nacional.
- Weimer, P., & Shipp, C. (2004). *Mass Transport Complex: Musing on Past Uses and Suggestions for Future Directions*.
- Winkler, W., Spikings, R., Villagómez, D., Egüez, A., Abegglen, P., & Tobler, S. (2002). The Chota Basin and its Significance for the formation of the Inter-Andean Valley in Ecuador. *Internatonal Symposium on Andean Geodynamic (ISAG)*, 5(1), 705–708.
- Winkler, W., Villagómez, D., Spikings, R., Abegglen, P., Tobler, S., & Egüez, A. (2005). The Chota basin and its significance for the inception and tectonic setting of the inter-Andean depression in Ecuador. *Journal of South American Earth Sciences*, 19(1 SPEC. ISS.), 5–19. <https://doi.org/10.1016/j.jsames.2004.06.006>
- Winter, T. (1990). *Mécanismes des déformations récentes dans les Andes équatoriennes*.